University of Southern Queensland

Faculty of Health, Engineering & Sciences

Circuit Breaker Simulated Operation & Behaviour Under Faulted Power System Conditions

A dissertation submitted by

B. Wentworth

in fulfilment of the requirements of

ENG4112 Research Project

towards the degree of

Bachelor of Power Engineering

Submitted: October, 2016

Abstract

The rapid increase in electrical demand and supply reliability for both domestic and industrial use throughout the modern world provides a set of unique challenges for supply authorities. It is not only paramount that the ever increasing supply and reliability demands are met but also environmental and cost concerns are addressed.

It has been proven that single pole tripping and reclosure schemes implemented on EHV (Extra High Voltage) transmission lines greatly aid in both supply availability and reliability. However, it is obvious that such schemes will greatly increase the complexity to both the primary and secondary systems. Subsequently, it is clear that the behaviour of the primary network under single pole operation must be extensively modelled to enable adequate protection and control by secondary protection systems.

Throughout the following study a technique for determining the maximum fault duration on a transmission network that incorporates single pole tripping has been developed. Further to this, investigations into accurate modelling of the physical network particularly pertaining to the fault arc that will be seen inside an EHV circuit breaker when opening under faulted network conditions has been undertaken. These techniques have been utilised to produce a specific maximum fault duration of 57ms for an example case study; subsequent circuit breaker failure times were then developed for a number of protection devices.

University of Southern Queensland
Faculty of Health, Engineering & Sciences

ENG4111/2 *Research Project*

Limitations of Use

The Council of the University of Southern Queensland, its Faculty of Health, Engineering & Sciences, and the staff of the University of Southern Queensland, do not accept any responsibility for the truth, accuracy or completeness of material contained within or associated with this dissertation.

Persons using all or any part of this material do so at their own risk, and not at the risk of the Council of the University of Southern Queensland, its Faculty of Health, Engineering & Sciences or the staff of the University of Southern Queensland.

This dissertation reports an educational exercise and has no purpose or validity beyond this exercise. The sole purpose of the course pair entitled "Research Project" is to contribute to the overall education within the student's chosen degree program. This document, the associated hardware, software, drawings, and other material set out in the associated appendices should not be used for any other purpose: if they are so used, it is entirely at the risk of the user.

Certification of Dissertation

I certify that the ideas, designs and experimental work, results, analyses and conclusions set out in this dissertation are entirely my own effort, except where otherwise indicated and acknowledged.
I further certify that the work is original and has not been previously submitted for assessment in any other course or institution, except where specifically stated.

B. Wentworth
0061038774

Acknowledgments

First and foremost I would like to thank my supervisor Dr Tony Ahfock for his unwavering support and assistance throughout the entire dissertation process; without his invaluable assistance the completion of this dissertation would not have been possible.

Secondly, I would like to thank my family; Heather, Greg, Megan and Laura for the support and encouragement shown when the demands of this dissertation appeared too great.

B. Wentworth

Contents

List of Figures

List of Tables

Chapter 1

Introduction

The following chapter is comprised of three sections; firstly, the justification and reasoning behind the need for this dissertation are discussed, secondly, the overall objectives are outlined and described, and finally, the prerequisites will be defined.

1.1 Project Justification

As global population and standard of living continue to rapidly increase it is obvious and indisputable that the demand for electricity will also continue to increase. In addition to this consumption accretion both household and industrial consumers are also expecting an ever increasing level of supply reliability.

In many cases these large increases in demand will put additional strain on aging power system equipment that is already heavily loaded. This will evidently reduce the level of reliability achieved.

The foremost solution would be to install additional transmission and distribution equipment that achieve very high levels of system redundancy. However this solution is not practicable for two main reasons: firstly, society's ever increasing environmentalist influence demands the reduction in destruction of flora; secondly, the increase in construction costs predominantly driven by inflation and the rise of wages have imposed heavy economic restrictions on many distribution and transmission companies.

The above restrictions have subsequently forced many distribution and transmission companies to seek and develop technologies that can supply large amounts of reliable power using fewer transmission lines, which will thereupon reduce both environmental damage and costs.

In an attempt to meet the requirements and restrictions outlined above, transmission companies must essentially have fewer transmission lines that are capable of supplying very large amounts of power. This is achieved by installing EHV (Extra-High Voltage) lines which become backbones to the electricity network.

As the amount of power transported by these network backbones is so great it is abundantly clear that additional reliability measures must be taken to prevent mass outages in the case of an unexpected system event. This additional reliability on the EHV network is often achieved by the application of single pole tripping.

Although single pole tripping increases reliability it also important to note that it greatly increases the complexity of system events and related protection and control devices.

It is clear from the above paragraphs that there is a need to determine, understand and model the behaviour of three phase networks that operate with a single pole tripping scheme.

1.2 Objectives

The overall aim of this dissertation is to give a detailed study of single pole circuit breaker operation and arcing characteristics under faulted power system conditions. Arcing characteristic models will be combined with power system network models for the purpose of determining the realistic clearance time for a high voltage circuit breaker, from fault initiation to fault clearance under various network configurations/conditions; subsequently applying these findings to a three phase network where minimal clearance and circuit breaker failure times are required to ensure network stability. The six following points outline the main project objectives.

A) Examine existing information on EHV (Extra High Voltage) CB (Circuit Breaker) fault modelling/data and review for applicability.

B) Determine the characteristics of three (3) phase (single pole operated) EHV CBs.
C) Utilise EHV CB models to simulate a power network that can achieve the single pole tripping characteristics defined in objective B
D) Determine a realistic fault characteristic for a single phase fault in a three phase power system.
E) Utilise a realistic arc model under various system faulted conditions.
F) Analyse fault clearance times to determine a realistic circuit breaker failure time.

1.3 Resource Requirements

The network simulation including all EHV CB arc modelling and fault modelling is to be implemented using Mathworks Simulink Simscape Power Systems. Existing Mayr and Cassie arc models were available from Mathworks(a) (2016).

1.4 Chapter Summary

This introductory chapter has provided the justification and project objectives. Firstly the increase in consumer demand and reliability expectation was discussed; this subsequently led into the justifications behind utilising single pole tripping schemes rather than installing new transmission and distribution equipment. Secondly, the overall aim and project objectives were discussed to ensure a clear and concise dissertation direction.

Chapter 2

Background

The following chapter is comprised of two main sections; technical background and fault data. The first section describes the operational behaviour of a single pole scheme and gives a detailed example of the improvements seen when using a single pole network; the second section contains a record of a single phase to ground fault that is to be used extensively to determine EHV CB characteristics and parameters.

2.1 Technical Background

Throughout the following section a discussion focusing on the behaviour and characteristics of a single pole circuit breaker utilised within a three phase network will be undertaken; this dialogue will contribute towards meeting the requirements of objective B. Furthermore, an in-depth investigation and subsequent case study into the effect single pole circuit breakers have on network stability will be carried out.

2.1.1 Circuit Breaker Operation

A protection and control scheme that incorporates single pole tripping will initially detect a fault within the protected object or zone as per any standard 3 pole scheme. However after this initial fault detection the protection device will then determine what type of fault is occurring and the number of phases involved. If it is determined that a phase to ground fault has occurred then a protection trip will be issued to the faulted phase only,

leaving the remaining two phases closed and supplying load. When a two phase or three phase fault is detected then a protection trip will be issued to all poles.

It is important to note that whenever a single pole trip is issued a re-closure initiate for that pole is also issued as the network is not designed to run on two phases alone; the reasoning behind this will be discussed and justified in detail later in this section.

As a generalised statement single pole schemes will use the below pro forma;

Single phase fault: the faulted phase is tripped and reclosed after a pre-defined dead time. If the fault has been cleared then the system returns to stable conditions. If the fault has not cleared after this dead time then the remaining two phases will be tripped. This will cause both a single pole and three pole reclose lockout. It is also important to implement a single pole circuit breaker fail scheme. In this scenario a single pole trip has been issued and the pole has not opened; after a predetermined breaker failure time a three pole trip must be issued to the original circuit breaker and the backup breaker/s upstream. The variation from a normal breaker failure scheme is that even under correct operation of a single pole trip the remaining two phases will continue to carry load current. Because of this load current each pole must have an individual current check to correctly assess the breaker failure conditions.

Two phase and three phase faults will trip all three poles and will be reclosed after a predetermined dead time. If the fault has been cleared then the system returns to stable conditions. If the fault has not cleared after this dead time then all three poles will be tripped and no further reclosure will take place. As per any three pole scheme if a trip is issued and the fault has not been cleared within a pre-determined time circuit breaker fail initiate will be issued.

Evolving faults must also be given consideration when implementing single pole tripping. Evolving faults start as a single phase to ground fault and then involve other phases before that fault is cleared. As single pole protection schemes have protection on a per pole basis they will inherently have some capability to deal with faults evolving; however additional logic is required to ensure that a three pole trip is issued when the second individual pole fault detector is active. This is a built in function in almost all modern relays that support single pole tripping.

2.1.2 Network Stability

Ngamsanroaj & Watson (2014) state that over 90% of transmission line faults are phase to ground and transient. Following this reasoning it is of no surprise that modern power networks implement single pole tripping schemes. These schemes are utilised to increase the reliability and availability of mesh transmission systems. It is blatantly obvious that the degree of which single pole tripping can improve the reliability of a mesh network is dependent on how that particular mesh network is configured.

In any case single pole tripping will increase the reliability of any network as when a single pole is tripped the increase of network impedance is much less than that of a three pole trip. AEMO (2013) show that the Victorian transmission network has a 500kV backbone that not only runs the entire length of the state but also interconnects with South Australia and New South Wales. It is obvious that such a intergral component of the transmission network will require the highest level of reliability available; this backbone has two parallel 500kV lines that implement single pole tripping at all terminal locations. Utilising the methodology outlined in GE Group (2002) in combination with the network parameters obtained from the Victorian transmission authority the following example will demonstrate the necessity for single pole tripping within the EHV Victorian mesh network.

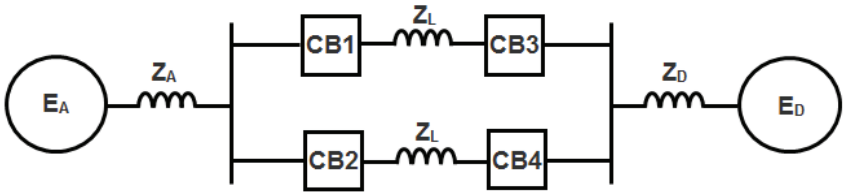

Figure 2.1: Simplified Network Impedance Diagram.

Figure 2.1 can be considered a simplified version of a section within the Victorian backbone. The maximum power that can be delivered can be easily obtained by:

$$P_{MAX} = \frac{E^2}{X} \tag{2.1}$$

Where P_{MAX} is the maximum power the network can deliver, E^2 is the constant system voltage and X is the sum of the line and machine reactances across the path.

Equation 2.1 is the theoretical steady state stability limit, and will occur when the voltage at source E_A leads the voltage at source E_D by 90 degrees. It is widely known that networks do not operate at the steady state stability limit. Equation 2.1 can be expanded into 2.2 to represent a more realistic power transfer across the system.

$$P = \frac{E_A E_D}{X_{AD}} Sin(\delta) \tag{2.2}$$

Where E_A is the phase to phase transmission voltage at A, E_D is the phase to phase transmission voltage at D, X_{AD} is the system reactance between A and D, finally δ is the angle E_A leads E_D.

Due to the heavy level of voltage regulation throughout the network we can assume that the voltages at source A and D are held constant. This gives a relationship where the angle between the two voltages is directly related to the power flow. The higher the system reactance, the higher the angle between the two voltage sources. Hence as described above the lower the change of system reactance the greater the stability of the system.

For the purposes of this example the following assumptions have been made: the line characteristics of line B and line C are identical ($Z_B = Z_C = Z_L$), impedance Z_A is equal to 20km of the total line impedance for one line and impedance Z_D is equal to 10km of the total line impedance for one line.

The following data about a specific section of the Victorian 500kV network has been obtained from the transmission authority: positive sequence impedance for entire line as 39.57Ω, zero sequence impedance for entire line as 112.02Ω and the line length as 146km. Hence $Z_{L1} = 39.57\Omega$ and $Z_{L0} = 112.02\Omega$. Subsequently the following can easily be obtained:

$$Z_{A1} = 20 * \frac{Z_{L1}}{l} \tag{2.3}$$

$$Z_{A0} = 20 * \frac{Z_{L0}}{l} \tag{2.4}$$

$$Z_{B1} = 10 * \frac{Z_{L1}}{l} \tag{2.5}$$

$$Z_{B0} = 10 * \frac{Z_{L0}}{l} \tag{2.6}$$

Where l is the 146km length of the line.
Using equations 2.3, 2.4, 2.5 and 2.6 we can determine Z_{A1} as $5.4200\Omega/km$, Z_{A0} as $15.3460\Omega/km$, Z_{B1} as $2.7100\Omega/km$ and Z_{B0} as $7.6730\Omega/km$.

$$Z_{AD-Normal} = Z_{A1} + \frac{Z_{L1}}{2} + Z_{D1} \tag{2.7}$$

Equation 2.7 shows the effective impedance between the two sources under normal operational conditions and can easily be determined as 27.9150Ω.

$$Z_{AD-Single-Line} = Z_{A1} + Z_{L1} + Z_{D1} \tag{2.8}$$

Equation 2.8 describes the effective impedance between the two sources with one line in service. This situation would occur when a three pole trip has occured on one of the lines with the other remaining in service. Equation 2.8 can be determined that $Z_{AD-Single-Line}$ is equal to 47.7Ω.

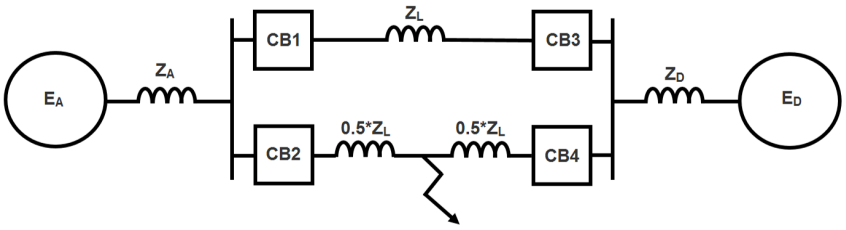

Figure 2.2: Simplified Network Impedance Diagram - Fault Location.

Now consider Figure 2.2 which indicates a single phase to ground fault in the centre of one of the transmission lines. When analysing a phase to ground fault positive, negative and zero sequence networks must be be analysed.

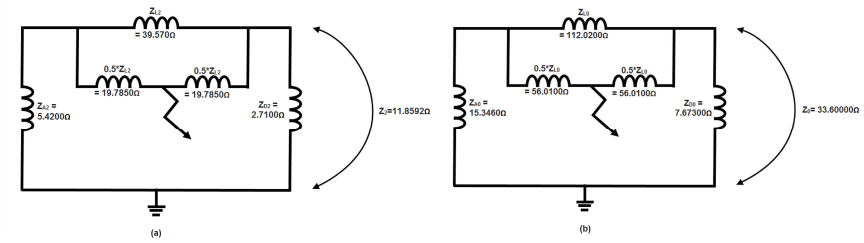

Figure 2.3: (a) Negative Sequence Diagram. (b) Zero Sequence Diagram

Figure 2.3 (a) shows the negative sequence impedances, using delta-star transformation

and series reduction the negative sequence impedance can be reduced to a single value of 11.8592Ω. While Figure 2.3 (b) shows the negative sequence impedances, using delta-star transformation and series reduction the negative sequence impedance can be reduced to a single value of 33.6000Ω

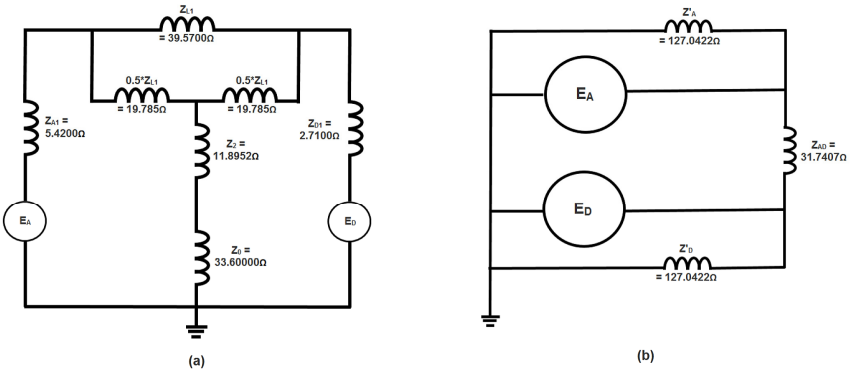

Figure 2.4: (a) Combined Sequence Diagram.(b) Simplified Combined Sequence Diagram

Figure 2.4 (a) shows the combined sequence diagram. This diagram incorporates all three sequence networks; however it must be simplified to be of any real use. Performing successive star delta transformation in combination with series reduction on Figure 2.4 (a) we can obtain Figure 2.4 (b). As Figure 2.4 (b) shows the combined sequence impedance can be simplified down three values, however as we are attempting to determine the impedance between the sources it is clear that we only require Z_{AD} which has been simplified to 31.7407Ω. In this instance we will assume that the resistive component is negligible, hence; $Z_{AD} = X_{AD}$

Using equation 2.2 the table 2.1 can be created:

Table 2.1: Summary System δ With Respect to System Impedance Change.

Case	Z_{AD}	δ
2 lines in service (normal conditions)	25.92 Ω	24.50°
2 lines in service (A-G fault - 1 pole trip)	31.74 Ω	30.52°
2 lines in service (A-G fault - 3 pole trip)	47.70 Ω	49.75°

Using the simplified equal area stability equations determined in GE Group (2002) we get the following stability equation:

$$\frac{E^2}{X_b}(Cos(\delta_2) + Cos(\delta_1)) > P_T(\pi - \delta_1 - \delta_2) \tag{2.9}$$

Where E is the constant system voltage, X_b is the system impedance after breaker operation, δ_1 is the angle of the system before the breaker operation, δ_2 is the angle of the system after the breaker operation and P_T is the total power flowing through the system at the time of the breaker operation.

Table 2.2 can be developed by applying equation 2.9 to each of the circuit breaker operation scenarios. Equation 2.2 has been used to determine a realistic power flow of 4000 MW at the time of fault.

Table 2.2: Summary of System Stability With Respect to δ.

Case	Equation Results	System
2 lines in service (A-G fault - 1 pole trip)	13952 MW > 8725 MW	Stable
2 lines in service (A-G fault - 3 pole trip)	8156 MW > 7383 MW	Stable

Whilst it can be seen that under the given conditions the system will remain stable for both a single pole and three pole trip, it is clear that the system maintains a much higher level of stability for a single pole trip. It is also important to note that if the system were to be subjected to above normal loading conditions then a three pole trip on one line may result in the system becoming unstable.

2.2 Fault Data

Fault records obtained from the Victorian 500kV transmission network will be used to obtain numerous parameters for the simulated network. By obtaining parameters from actual fault data a more realistic model can be produced using less assumptions, this will aid in meeting objectives B and D. The fault oscillogram in figure 2.5 has been extracted from a recording device that was monitoring a 550kV, 63kA, 50Hz circuit breaker. This type of breaker is used extensively throughout this and many other EHV networks.

The values obtained from the fault oscillogram will be measured and used for validation and verification of the calculated fault model used within this study. Figure 2.5 is a captured fault record of a single phase to ground fault on the Victorian EHV network and is suitable for the purposes of this study as all simulated faults are of a single phase to ground nature.

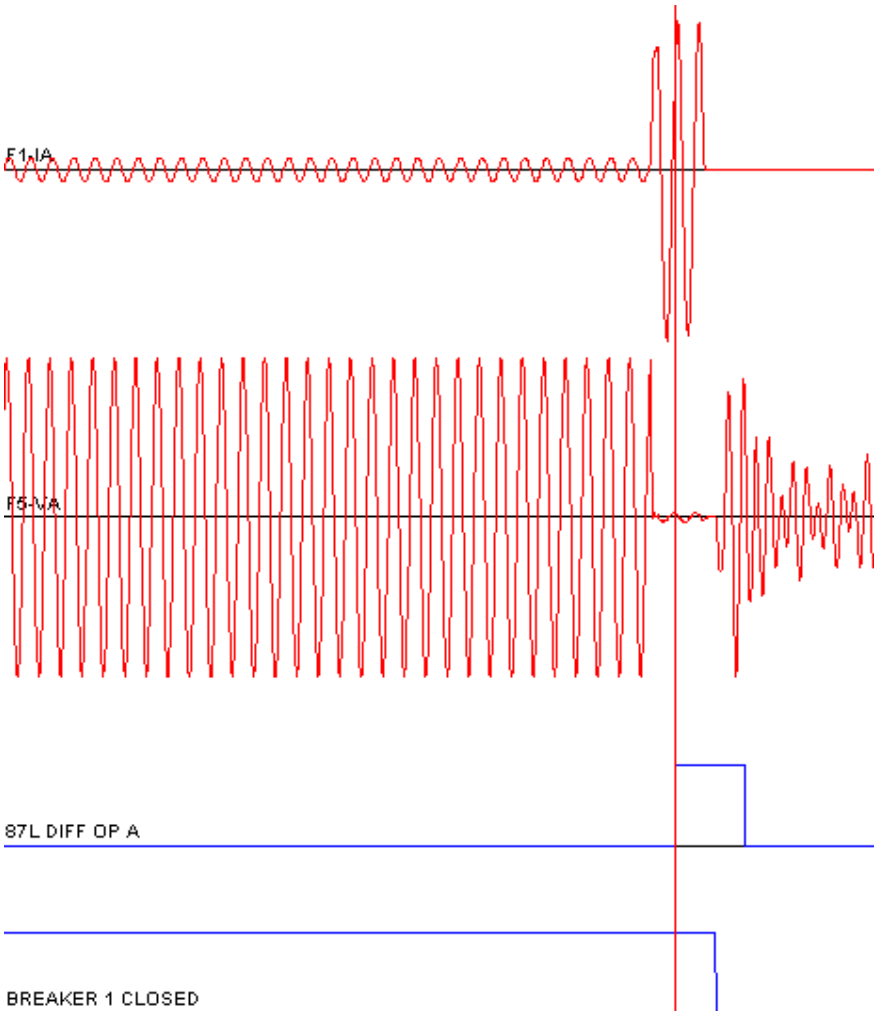

Figure 2.5: Fault Oscillogram (Courtesy Sing Wai Mak, Ausnet Services).

It can readily be seen that the fault oscillogram in Figure 2.5 comprises of four components; F1-A shows the recorded A phase faulted line current, F5-VA indicates the A phase faulted line voltage, 87L DIFF OP A illustrates when the differential protection element operated and BREAKER 1 CLOSED describes the A phase CB closed status.

The current zero for this fault occurs 53.13 ms after fault inception and 29.38 ms after protection relay operation.

2.3 Chapter Summary

The background chapter is comprised of two major sections; the first section contains a technical background and provides a detailed example of the benefits seen when utilising single pole tripping within a three phase network. The second section provides a fault

record from an in service protection device that has been subject to a single phase to ground fault; this record will be utilised within later chapters to establish realistic circuit breaker parameters.

Chapter 3

Literature Review

The following section is an overview of the literature used to determine the characteristics and behaviour of SF_6 CB's within an EHV network. This section will address the behaviour of extra high voltage circuit breakers particularly pertaining to arcing during faulted network conditions. It is the aim of the report to use these previous studies as a benchmark for determining methods to obtain realistic fault simulation and subsequently fault clearance times.

3.1 Circuit Breaker Characteristics

The following section discusses the characteristics of an EHV CB; subsequently it is an important component in meeting the requirements of objective B. Firstly it is important to consider how and why an EHV CB will operate. When a fault occurs on an EHV network a protective device will detect the faulted condition and then initiate a trip to the EHV CB. This trip initiate will effectively begin the process of parting of the EHV CB contacts. Whilst the time taken for the CB contacts to physically part is extremely quick (a matter of milliseconds) it is still long enough for an arc to form. There are numerous types of insulation materials used by manufacturers of EHV CB's; however the current leader in insulation material is SF_6. Subsequently this study will focus on EHV CB's that use SF_6 as an insulating gas.

Oh, Y. and Song, K. (2015) describe that when analysing current interruption in SF_6 CB's it is important to consider the arc plasma generated between the separating contacts. This plasma will be at a temperature of many thousands of degrees, encompass high electric field conduction as well as super and sub sonic gas flows . The aforementioned factors all hinder in the extinguishing of the arc. With this in mind the overall concept of arc extinction is still relatively simple; the arc resistance increases as the contacts part, when this arc resistance is large enough the arc current is interupted, this is particularly prevalent at the zero crossing. Conversely if the resistance is not large enough directly after a zero crossing occurs the arc will be re-ignited and the fault will continue.

3.2 Transmission Line Characteristics

To determine which line parameters are necessary to accurately model a single phase to ground fault we must first look at how the line will behave under faulted conditions; these line characteristics will aid in meeting the requirements of objective A and B. Jannati, Vahidi, Hosseinian & Ahadi (2011) describe that when a system is healthy and a phase to ground fault occurs two distinct arcs will be seen, a primary arc and a secondary arc.

The Primary arc is essentially caused by a short circuit that has been formed when one phase of a healthy system is faulted to earth. Arc quenching will be discussed in much greater detail throughout this report; however for the purpose of determining line parameters the primary arc can be considered quenched when the contacts of the high voltage circuit breaker on the faulted phase are fully opened. After the aforementioned primary fault has been cleared by the operation of the high voltage circuit breaker it will be assumed that the two non-faulted phases will remain closed and supplying load. Jannati et al. (2011) state that due to the two healthy phases remaining closed a capacitive coupling effect will be seen and the faulted phase may then produce a secondary arc.

It is well known that to effectively model any electrical circuit the impedance must be known, transmission lines are no exception. However, as justified in the above paragraphs, to accurately model a line with single pole tripping it is not only essential to have accurate line impedance values but effectively represent the capacitive coupling effect.

Pinto, Costa, Kurokawa, Monteiro, de Franco & Pissolato (2014) describe in great detail how overhead tranmission line characteristics are directly related to the length of the line

and also the spacing between conductors; in particular how multiconductor transmission systems can be represented by an impedance matrix [Z] and admittance matrix [Y]. However they continue to describe that whilst maintaining sufficient accuracy these two multiconductor matrix's can be simplified into four sequence component value; positive sequence capacitive reactance (X_{C1}), zero sequence capacitive reactance (X_{C0}), positive sequence impedance (Z_1) and zero sequence impedance (Z_0).

3.3 Network Fault Levels

To accurately and effectively model any fault and meet the requirements of objective B and C it is important to determine the perspective maximum short circuit level at that particular point in the network. These short circuit levels are expected to be much larger than the network has been designed to handle continuously. Perspective maximum short circuit levels are determined by the voltage and the impedance of the system and are essentially considered as the maximum amount of current that can be delivered at the specified point in the network.

The 500kV network that has been used for validation throughout various stages of this report is a critical component to the Victorian transmission network; AEMO (Australian Energy Market Operator) have publically released the short circuit fault values for all major terminal stations throughout the entire Victorian backbone. The relevant short circuit values from AEMO (2012) have been summarised in table 3.1.

Table 3.1: Short Circuit Ground Fault Levels.

Station	Pre-Fault Voltage	I_g	Deliverable Power
MLTS	520.6 kV	15.5 kA	8069.3 MVA
MOPS	527.5 kV	9.5 kA	5011.3 MVA
TRTS	526.0 kV	7.5 kA	3945.0 MVA
APD	520.5 kV	8.8 kA	4580.4 MVA
HYTS-B1	523.6 kV	8.5 kA	4450.6 MVA
HYTS-B2	523.8 kV	8.7 kA	4557.1 MVA

3.4 Network Loading Effects

Goday, E. and Celaya, A (2012) describe how a three phase transmission line will be subjected to both electromagnetic and electrostatic coupling during its normal operational conditions. It is subsequently obvious that these coupling effects will remain whenever all, or part of the transmission line is energised. Hence, it is clear that to achieve objective C these coupling effects must be considered in detail.

As described previously, when a single phase to ground fault occurs a primary arc is formed. The protection device will then initiate a single pole trip on the faulted phase. The un-faulted phases will remain closed and continue to supply load. It is because of this load voltage and current within the two un-faulted phases that electromagnetic and electrostatic coupling induce a voltage and subsequent current on the now open phase.

Electrostatic coupling is commonly called capacitive coupling and can essentially be described as a function of the line voltage and physical line characteristics. The line capacitance is a combination of the distance between each of the phases and also the distance of the phase conductors to the ground.

Goday, E. and Celaya, A (2012) have developed equation 3.1 to determine the electrostatic secondary arc current and equation 3.2 to represent the recovery voltage.

$$I_{ARC-C} = V_{LN} * j\omega C_m \tag{3.1}$$

$$V_{REC} = V_{LN} \frac{C_m}{(2C_m + C_g)} \tag{3.2}$$

Where V_{LN} is the line to neutral voltage, C_m is the equivalent capacitance between phases and C_g is the capacitance to ground. From the relationship defined in 3.2 it is easy to see that higher line voltages will produce higher levels of electrostatic coupling.

NTT Technical (2007) describe that electromagnetic induction is caused by alternating current inducing a magnetic field around the conductor it is flowing through. When another conductor is within this induced magnetic field it will then be subjected to the electromagnetic coupling effect. Horton, Halpin & Wallace (2006) go into great detail

describing how electromagnetic induction is a function of the load current and the total distance that the conductors are paralleled. In the situation of a single phase trip the conductors will obviously be parallel for the entire lenth of the line.

From the above paragraphs it is clear that the line voltage and current in the un-faulted phases will create an electrostatic and electromagnetic coupling effect in the recently opened faulted phase. It is clear that the larger the voltage and current of the un-faulted phases the larger the coupling effect. Hence loading on the transmission line will play a large role in the TRV (transient recovery voltage) seen.

3.5 Definite Maximum Fault Time

Clearly it would be ideal if the detection of a fault by a protective device and the operation of a high voltage circuit breaker happened instantaneously; however, in reality neither of these hold true.

When considering the realistic operation time to clear a faulted circuit, it is first important to consider what actually causes the interruption of current. The actual interruption device is a EHV CB. However for this interruption to occur a protective device must first initiate the operation. When a fault is present and detected by a protective device it will issue a trip to the EHV CB. Although both protection operation and EHV CB operation speeds are increasing as technology advances both of these aspects still take some physical time to complete and cannot be considered instantaneous.

It can then be said that with a very simplistic view when a EHV CB's contacts are fully open that any fault that was present will be cleared. For the purpose of this section of the study it will be assumed that the EHV CB's are of adequate rating to interrupt any fault and that all faults will be cleared when the circuit breaker contacts are fully open. With this assumption in mind the time of the fault is then limited to the initial detection time of the protection device plus the time it takes for the contacts of the EHV CB to fully open. This time will be called the definite maximum fault time. In reality, the fault may be broken before this time or not at all; earlier arc interruption will be discussed in later sections in great detail.

3.6 Arc Models

Literature relating to two prominent arc models will be discussed throughout the following section. In the first subsection Mayrs arc model will be analysed; the second will discuss Cassies arc model. To meet objective D it is the intent of this study to perform analysis using both arc models with the desire to then compare the results.

3.6.1 Mayr Arc Model

Schavemaker & van der Slui (2000) defines the Mayr arc as equation 3.3, where G is the arc conductance, u_m is the arc voltage, i_m is the arc current, τ_m is the arc time constant and P_0 is the cooling power.

$$\frac{1}{G}\frac{dG}{dt} = \frac{dlnG}{dt} = \frac{1}{\tau_m}(\frac{u_m * i_m}{P_0} - 1) \tag{3.3}$$

The Mayr model assumes that the thermal conduction at small currents is the cause of power loss. It can then be said that the arc conductance is highly temperature dependant. Further to this it can be determined that the arc conductance depends very little on the cross sectional area; subsequently the cross sectional area of the arc will be assumed as a constant. In addition to the above assumptions Mayr states that the relationship between the voltage and current is constant; hence P_0 is equal to P_{LOSS} and is to be considered constant. When there is no power input to the arc (zero crossing) τ_m is time constant of the change in temperature.

$$P = ui \tag{3.4}$$

Using the fundamental relationship in equation 3.4 we can simplify equation 3.3 to obtain 3.5:

$$\frac{1}{G}\frac{dG}{dt} = \frac{dlnG}{dt} = \frac{1}{\tau_m}(\frac{P}{P_{LOSS}} - 1) \tag{3.5}$$

By inspection of equation 3.3 and 3.5 it is clear that P can be determined and will vary

throughout the iterative process, however P_{LOSS} is a constant that must be known prior.

3.6.2 Cassie Arc Model

Bizjak, Zunko & Povh (1995) defines the Cassie arc as equation 3.6, where U_c is the arc voltage and τ_c is the arc time constant.

$$\frac{1}{G}\frac{dG}{dt} = \frac{1}{\tau_c}(\frac{u^2}{U_c^2} - 1) \tag{3.6}$$

The Cassie model assumes that convection is the only cause of power loss in the arc. Subsequently it can assumed that the temperature in the arc is constant. Further to this it can be determined that the cross sectional area of the arc is proportional to the current.

By inspection of equation 3.6 it is clear that u can be determined and will vary throughout the iterative process, however U_c is constant and must be known prior.

3.7 Arc Conductance

It is quite obvious that the breaking ability of a circuit breaker will depend on a multitude of factors. Subsequently there are a number of ways to successfully model circuit breaker arcing. Smeets & Kertsz (2000) have previously determined that arc conductance at current zero is an exceptional parameter for determining the ability of a circuit breaker to interrupt current and subsequently aid in meeting objective D.

Summarising the investigation performed by Smeets & Kertsz (2000) they determine that large power losses will increase the ability of current interuption; after consideration of this statement is also quite intuitive.

It is easy to see that large power loss is directly related to small arc conductance; this is obvious because conductance is the reciprical of resistance. Hence, if either the resistance or conductance is determined then the other is easily obtained.

3.8 Fault Impedance

Andrade,V and Sorrentino, E (2010) explain that the magnitude of the short circuit current that is seen will be dependent on the fault impedance. Upon thinking about this, it is actually an incredibly simple realisation; the relationship of $V = IZ$ must hold true; hence, when an impedance is high, the current must be low.

It is important to remember that the total fault impedance is made up of three major components; the arcing resistance across the circuit breaker, transmission line tower grounding, and any additional object that may have caused the faulted condition. If an object has come into contact with a transmission line and caused a fault it can have almost any combination and variation of impedance. However Jeerings & Linders (1989) define that the most common causes are either highly resistive or those of essentially of zero resistance.

3.9 Chapter Summary

The literature review has collected and complied relevant information from various sources to produce a realistic expectation of a single pole operated SF_6 CB within a three phase EHV network. The behaviour and effects of numerous interconnected power system components were discussed at length to provide a comprehensive understanding of the overall system. Further to this, particular attention has been given to internal CB arcing that would be seen under faulted network conditions. It is abundantly clear that both the network and circuit breaker characteristics determined within this chapter are essential to successfully completing the remaining dissertation objectives.

Chapter 4

Methodology

The following chapter will discuss the methodology used to simulate a single pole trip on a three phase network. Circuit breaker arcing models and power system modelling components will also be outlined throughout this chapter. The selection and reasoning of the network modelling components, definite maximum fault time characteristics, Mayr arc model parameters, Cassie arc model parameters, fault impedance considerations, fault location variations and fault inception angle alterations will be discussed.

4.1 Simulink Model Introduction

Due to the complexity and sheer number of calculations required to accurately reflect a power network it was decided that the use of simulation software would be necessary. Mathworks Simulink Simscape Power Systems was the obvious package of choice as this software package has been used on numerous occasions throughout studies at USQ and would satisfactorily contribute to meeting objective C. The below subsections have been created to show how the components of the simulation model were developed.

4.1.1 Line Parameters

For purposes of this study the line parameters have been obtained from the network authority and hence they will not be verified from first principles. To coincide with the technical introduction the parameters obtained are for the same 146.7300km transmission

line. The following values are for the full length of the line; Positive sequence capacitive reactance (X_{C1}) of 1621.2000Ω, Zero sequence capacitive reactance (X_{C0}) of 3117.1000Ω, Positive sequence impedance (Z_1) of 2.9819+39.4536jΩ, Zero sequence impedance (Z_0) of 18.2598+110.5194jΩ.

To accurately reflect the transmission line it is important to determine the positive and zero sequence resistance in per unit length (ohms/km), positive and zero sequence inductance per unit length (H/km) and positive and negative sequence capacitance per unit length. Using basic principles all of the per unit line parameters can be obtained from the aformentioned values provided by the network authority.

$$C_1 = \frac{1}{2\ \pi\ f\ X_{C1}} / l_{LINE} \tag{4.1}$$

$$C_0 = \frac{1}{2\ \pi\ f\ X_{C0}} / l_{LINE} \tag{4.2}$$

$$R_1 = \frac{2.9820}{146.7300} \tag{4.3}$$

$$R_0 = \frac{18.2598}{146.7300} \tag{4.4}$$

$$L_1 = \frac{Z_1}{2\ \pi\ f} / l_{LINE} \tag{4.5}$$

$$L_0 = \frac{Z_0}{2\ \pi\ f} / l_{LINE} \tag{4.6}$$

Using Equations 4.1, 4.2, 4.3, 4.4, 4.5 and 4.6 the line parameters can be determined as follows: C_1 as $13.3812\eta F$, C_0 as $6.9595\eta F$, R_1 as 0.0203Ω, R_0 as 0.1244Ω, L_1 as $8.4473mH$ and L_0 as $2.3976mH$.

4.1.2 Line Modelling

Within the previous sub-section the line characteristics have been determined and it is now critical to decide how they can most effectively be used within Mathworks Simulink Simscape Power Systems. There are a number of equally valid approaches that could be utilised to simulate a long transmission line using the values determined above. For the purposes of this study it has been determined that two of the pre-built Simscape Power Systems block models may be suitable. The Three-Phase Pi Section Model and the Distributed Parameter Line model will now be discussed to decide which best meets the needs of the analysis being undertaken.

As the name indicates the three-phase pi section model implements parameters that are lumped into a pi arrangement. In this model the transmission line resistance, inductance and capacitance are lumped as shown in Figure 4.1.

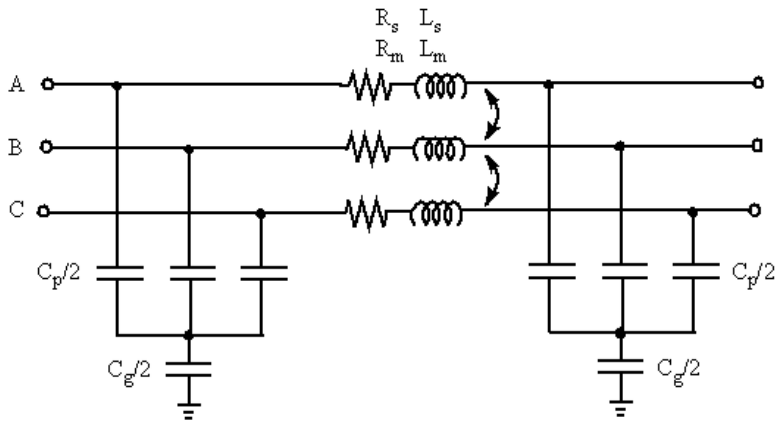

Figure 4.1: PI Line Model Diagram (Mathworks(b) 2016).

Throughout the study it is intended that the fault is to be moved to various locations along the line and subsequently it is seen that a model using distributed parameters would be beneficial. It is also important to note that throughout Mathworks Simulink Simscape Power Systems documentation it was stated the three-phase pi section model does not handle high frequency transients as well as the distributed parameter model.

As described by the name, the distributed parameter line model does exactly that; distributes the transmission line resistance, inductance and capacitance across the entire length of the line. It is important to note that although the line parameters are distributed, the losses are lumped. Figure 4.2 depicts a single phase representation of the distributed parameter line model. As the power system model used throughout this study

is a three phase system, the distributed line parameter block will automatically perform Modal Transformation to convert the individual phase values into Modal values that are independent.

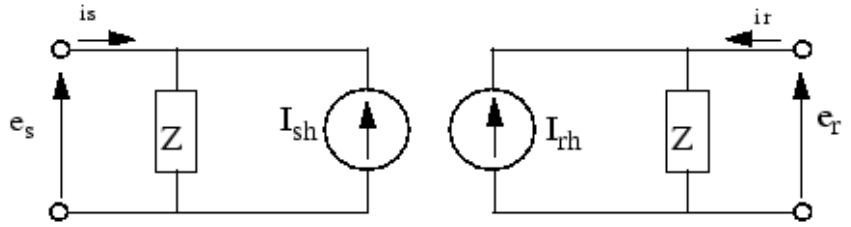

Figure 4.2: Distributed Parameter Line Diagram (Mathworks(c) 2016).

When reading technical documentation Mathworks(c) (2016) it states that the distributed line method uses Bergeron's traveling wave method and then defines the following equations for figure 4.2.

$$e_r(t) - Z_c i_r(t) = e_s(t-\tau) + Z_c i_s(t-\tau) \tag{4.7}$$

$$e_s(t) - Z_c i_s(t) = e_r(t-\tau) + Z_c i_r(t-\tau) \tag{4.8}$$

Given that;

$$i_s(t) = \frac{e_s(t)}{Z} - I_{sh}(t) \tag{4.9}$$

$$i_r(t) = \frac{e_r(t)}{Z} - I_{rh}(t) \tag{4.10}$$

As stated previously the losses will be lumped.

$$I_{sh}(t) = (\frac{1+h}{2})(\frac{1+h}{Z}e_r(t-\tau) - hI_{rh}(t-\tau)) + (\frac{1-h}{2})(\frac{1+h}{Z}e_s(t-\tau) - hI_{sh}(t-\tau)) \tag{4.11}$$

$$I_{rh}(t) = (\frac{1+h}{2})(\frac{1+h}{Z}e_s(t-\tau) - hI_{sh}(t-\tau)) + (\frac{1-h}{2})(\frac{1+h}{Z}e_r(t-\tau) - hI_{rh}(t-\tau)) \tag{4.12}$$

Where;

$$Z = Z_c + \frac{r}{4} \tag{4.13}$$

$$h = \frac{Z_c - \frac{r}{4}}{Z_c + \frac{r}{4}} \tag{4.14}$$

$$Z_c = \sqrt{\frac{1}{c}} \tag{4.15}$$

$$\tau = d\sqrt{lc} \tag{4.16}$$

Where r is the line resistance, l is the line inductance and c is the line capacitance all in per unit (km) values. It can be seen from the paragraphs above that the distributed parameter line model would be the suitable for use throughout this study.

4.1.3 Network Loading Parameters

As described within the literature review it is paramount that the loading conditions along the line are simulated to achieve a realistic electrostatic and electromagnetic coupling effect. Table 4.1 has been derived from the example power transferred within the technical introduction; the values within this table will be used within the modelling process. It will be assumed that the line voltage remains constant on the un-faulted phases.

Table 4.1: Example Line Loading Records.

	No Load	Moderate Load
Line Power	0 MW (Voltage Only)	2000 MW

It is important to note that the no load scenario in Table 4.1 will still have energisation current and voltage for the line, however the load will not be consuming any active or reactive power.

4.1.4 Short Circuit Fault Level

The short circuit values that were tabulated in table 3.1 within the literature review can easily be implemented in Simscape Power Systems using the pre-built three-phase source with R-L impedance block. The Mathworks documentation (Mathworks(c) n.d.) describes that you can enter the internal source characteristics either directly or indirectly with short circuit values and an $\frac{X}{R}$ ratio. Since the network values available are short circuit values the later option will be used to define the internal impedance of the source.

4.1.5 Network Overview

Throughout the methodology section the importance, selection and justification of the individual electrical network components have been discussed; however the relationship of these components to each other has not yet been established. The paramount need to correctly identify how these network components are connected and interact is obvious as the interactions between almost any of the components involved will alter the resultant fault.

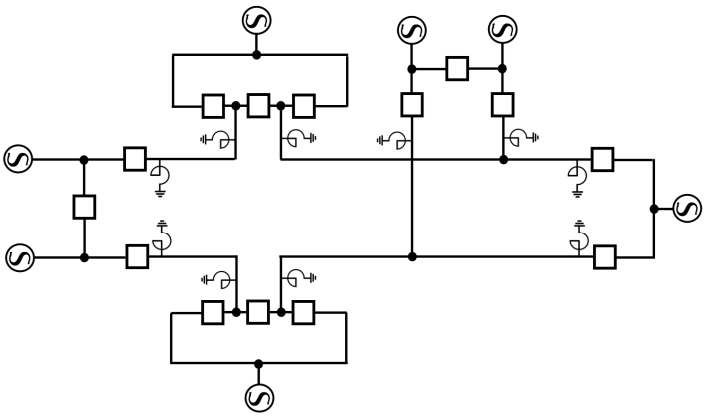

Figure 4.3: Simplified Network Diagram.

Figure 4.3 shows a simplified single line diagram of the network that is under analysis, whilst appendix F shows a detailed diagram of the Mathworks Simulink Simscape Power Systems model.

4.2 Definite Maximum Fault Time

To achieve accurate results and meet objective E utilising this method it is clear that the specific EHV CB times for CB's that are utilised within the particular section of network being analysed must be determined. Throughout the technical introduction a portion of the 500kV Victorian backbone was used; this portion of network will continue to be used to determine realistic values. The three EHV CB's that are used in this particular portion of the network are; Siemens 3AT5, ABB HPL550 T31A4 and Alstom GL317D. When consulting the technical documentation by Siemens (2008) it is specified that the Siemens 3AT5 trip time as 2 cycles (40ms), ABB (2014) specifies the ABB HPL550 T31A4 trip time as 2 cycles (40ms) and Alstom (2010) specifies the Alstom GL317D trip time is specified as 2 cycles (40ms).

Table 4.2: 500kV Circuit Breaker Recorded Operation Times.

CB Type	Fastest	Mean	Slowest
Siemens 3AT5	22 ms	31 ms	40 ms
ABB HPL550 T31A4	28 ms	37 ms	46 ms
Alstom GL317D	19 ms	31 ms	42 ms

As the majority of this equipment is aging, to accurately simulate the definite maximum fault time the actual operational times of in service protective devices have been summarised in table 4.3 and actual operational times of the extra high voltage circuit breakers have been summarised in table 4.2. These values have been obtained from utility maintenance records.

Table 4.3: 500kV Protection Device Recorded Operation Times.

Relay Type	Fastest	Mean	Slowest
GE L90	20.0 ms	24.5 ms	29.0 ms
MiCom P546	20.0 ms	25.0 ms	30.0 ms

Noting that the values in table 4.3 are the extremes of the protection relay; these values take into account the slowest and fastest protection elements regardless of protection type.

Table 4.3 gives the maximum protection relay operation time of 30.0 ms and Table 4.2 gives the maximum EHV CB operation time of 46 ms. Hence the definite maximum fault

time is 76 ms.

4.3 Arc Resistance & Conductance Calculation

It will be the aim of this section to determine the arc resistance at current zero for the recorded fault within the introduction; this will aid in meeting objectives B and D. As described within the literature review the arc resistance can essentially be determined using ohm's law.

$$R = \frac{v'}{i'} \tag{4.17}$$

Where v' is the gradient of the voltage and i' is the gradient of the current. Using Equation 4.17 it is easy to calculate the arc resistance at current zero; R_0 is described by 4.18.

$$R_0 = \frac{v'_{(arc-zero)}}{i'_{(arc-zero)}} \tag{4.18}$$

Where $v'_{(arc-zero)}$ is the voltage gradient as the time approaches current zero and $i'_{(arc-zero)}$ is the current gradient as time approaches current zero. Studies by Ahmethodzic, Kapetanovic, Sokolija, Smeets & Kertesz (2011) have previously indicated that the rapid changes at current zero can make these gradients very hard to determine. These studies have subsequently taken values immediately before current zero and found that they produce sufficiently acurate results. Hence the Equation 4.19 can be used to obtain the arc resistance 625ns before current zero. This study will use 625ns before current zero as it is the minimum step size available from the fault recording.

$$R_{625} = \frac{v_{(arc-zero-625ns)} - v_{(arc-zero)}}{625ns} \Big/ \frac{i_{(arc-zero-625ns)} - i_{(arc-zero)}}{625ns} \tag{4.19}$$

Using values obtained fom the fault record in combination with equation 4.19 it can be determined that R_{625} is 284.08Ω. For the purposes of this study R_{625} will be used.

4.4 Mayr Arc Model

The following section has been divided into two subsections and will contribute to meeting objective D and E; the first section discusses the methodology used to determine the Mayr arc model parameters, the latter section will then be used to discuss the implementation of the values determined former section.

4.4.1 Mayr Arc Model Parameters

Mathworks Simulink Simscape Power Systems (Mathworks(a) 2016) include a pre-built Mayr arc model which will be used extensively. Within the literature review it was found that we are required to know G and P_{LOSS}. There are a number of numerical methods to determine these values, however, the method that has been chosen for this report is to obtain the values from a previous fault record.

$$G = \frac{1}{R} \tag{4.20}$$

Using the basic relationship of equation 4.20 and the results from 4.19, G can easily be obtained as 3.52 mS.

$$P = ui \tag{4.21}$$

Using the fundamental power equation 4.21 and values u and i obtained from the aformentioned fault record at 625 ηs before zero current P_{LOSS} can be determined as 37.714 kW.

4.4.2 Mayr Arc Model Implementation

To solve the Mayr differential equation numerically, Gustavsson (2004) explains it must first be converted to discrete form. Following the method used by Gustavsson (2004) both sides of equation 3.5 will be multiplied by G; then the Euler forward approximation will be used to form the final equation 4.24.

$$\frac{dG}{dt} = \frac{1}{\tau_m}(\frac{i^2}{P_{LOSS}} - G) \tag{4.22}$$

$$\frac{G_{n+1} - G_n}{t_{n+1} - t_n} = \frac{1}{\tau_m}(\frac{i_n^2}{P_{LOSS}} - G_n) \tag{4.23}$$

Giving

$$G_{n+1} = \frac{\Delta t}{\tau_m}\frac{i_n^2}{P_{LOSS}} - G_n(1 - \frac{\Delta t}{\tau_m}) \tag{4.24}$$

The reciprocal of equation 4.24 will give you the arc resistance, this resistance is used to determine if the arc is extinguished.

4.5 Cassie Arc Model

The following section has been divided into two subsections and aims to contribute to objectives D and E; the first section discusses the methodology used to determine the Cassie arc model parameters, the latter section will then be used to discuss the implementation of the values determined former section.

4.5.1 Cassie Arc Model Parameters

Mathworks Simulink Simscape Power Systems (Mathworks(a) 2016) include a pre-built Cassie arc model which will be used extensively along side the Mayr model. Within the literature review it was found that U_c is constant and must be known prior. As to be expected, there are a number of numerical methods to determine this value, however, keeping alignment with previous sections U_c will be obtained from a previous fault record.

Similarly to the Mayr arc equation the arc conductance must be known; however this value will remain identical for both methods. Hence the equation 4.20 and the results from 4.19 remain true and G can easily be obtained as 3.52 mS.

U_c can easily be realised from the aformentioned fault record at 625 ηs before zero current and is determined as 307kV.

4.5.2 Cassie Arc Model Implementation

Similar to the Mayr arc equation to solve the Cassie arc equation numerically we must first convert it to discrete form. This can be done by multiplying both side of 3.6 by G. The Euler forward approximation will be used to form the final equation 4.27.

$$\frac{dG}{dt} = \frac{1}{\tau_c}(\frac{iu}{U_c^2} - G) \tag{4.25}$$

$$\frac{G_{n+1} - G_n}{t_{n+1} - t_n} = \frac{1}{\tau_c}(\frac{i_n u_n}{U_c^2} - G_n) \tag{4.26}$$

Giving

$$G_{n+1} = \frac{\Delta t}{\tau_c}\frac{i_n u_n}{U_c^2} + G_n(1 - \frac{\Delta t}{\tau_c}) \tag{4.27}$$

The reciprocal of equation 4.27 gives the arc resistance, this resistance is used to determine if the arc is extinguished.

4.6 Fault Location

Contributing to objective E a number of fault locations will be discussed throughout the following section. This study will focus in particular on three (3) positions along one (1) transmission line; the beginning of a transmission line, centre of a transmission line and finally at the end of a transmission line.

Figure 4.4 shows a single line diagram of the transmission network that will have the aforementioned faults applied to it. The TRTS-HYTS-APD transmission line was selected and is a three ended transmission scheme.

The three faults indicated in figure 4.4 (fault location 1, fault location 2 and fault location 3) will be applied and analysed individually.

As this network has two parallel transmission lines the beginning and end of the line fault simulations will have similar fault duration and behaviours, the major variation between

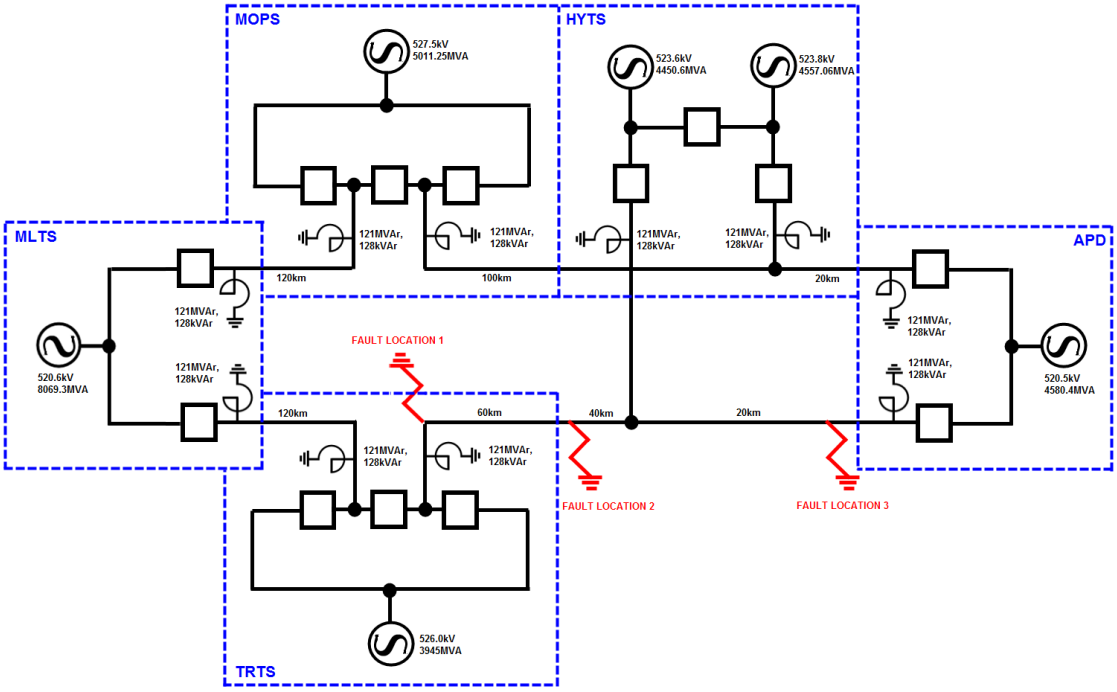

Figure 4.4: Single Line Diagram - Fault Locations.

them being the fault magnitude which is heavily influenced by the short circuit values of the closest terminal station.

The faulted condition in the middle of the transmission line will experience quite different behaviour to its two counterparts; in particular the TRV (transient recovery voltage) experienced will be much greater. This larger TRV is caused by the distance from the line reactors and electromagnetic and electrostatic effects produced be the long line length and will subsequently assist in the possibility of a restrike.

4.7 Fault Impedance

As discussed within the literature review, when an object comes into contact with a transmission line causing a fault it can have almost any combination and variation of impedance. However for the purpose of meeting objective E this study will consider the extreme cases of 0Ω impedance will be used for the low impedance simulated fault path and 1000Ω will be used for the high impedance simulated fault path.

As the fault circuit is simulated by closing an ideal circuit breaker to earth at the faulted location a variation in impedance will be achieved by adding a series resistance into the

fault circuit breaker.

4.8 Fault Inception Angle

Costa, Souza & Brito (2012) describe the fault inception angle as the electrical angle at which the fault occurs. This angle is taken at the faulted location and at the instant immediately before the fault occurs. As the faulted waveform is oscillating it is easy to see why the inception angle will have a major role in not only the duration of the fault but also the restriking characteristics seen.

Aiding in the successful completion of objective E this study will alter the faulted inception angle from -90° to 90° in steps of 30°. This alteration in inception angle can be achieved by varying the angle of the short circuit current in the three-phase source block. The inception angle will be taken at the fault location; hence, multiple sources and network parameters will be considered to achieve the correct angle at each faulted location.

4.9 Chapter Summary

The methodology chapter details the process and techniques utilised to successfully simulate a single pole trip on a three phase network. The selection, implementation, utilisation and justification of all individual network components and parameters including the Mayr and Cassie arc model were discussed in great detail.

Chapter 5

Results and Discussion

As described in detail throughout the methodology section Mathworks Simulink Simscape Power Systems was used to create a number of fault simulation models. Appendix F includes images of the nine (9) individual fault simulation models that were created to represent each arc simulation method at the various fault locations.

For each of the three (3) faulted locations eighty four (84) individual test states were simulated and results recorded. Appendix B, C and D include tabulated results for the varying combination of fault arc model, circuit impedance, system load, inception angle and fault location. A summary of the results obtained and subsequent discussion will be contained throughout the following section.

5.1 Results Summary

This section contains an overview of the results obtained whilst meeting objective E; the various combinations of faulted system conditions will be summarised whilst keeping a primary focus on the clearance time of the circuit breaker to enable the completion of objective F in the final section of this chapter. The longest fault duration summary Tables 5.1, 5.2 and 5.3 contain a succinct overview of Appendix B, C and D and show the longest simulated fault durations at the start, middle and end of the line respectively. These summarised tables not only include the fault duration for each of the three (3) different fault arc models at each location but also the system conditions under which

each fault duration was achieved.

Table 5.1: Results Summary - Start of Line - Table.

Model Type	Fault Impedance	Load (MW)	Max. Fault Duration (ms)	Inception Angle (°)	Fault Mag (A)	Post Fault Mag. (A)
DT	1000	0	99	0	236	49.1
Mayr	1000	0	46	-30	217	40.7
Cassie	1000	2000	43	-60	229	34.3

When considering Table 5.1 the fault current magnitudes from the various fault arc models indicate the peak faulted current in each scenario. Whilst these current magnitudes appear to be similar when arranged in this fashion, we must consider Tables 5.2 and 5.3 which show large variances in the fault and post fault current magnitudes when comparing the arc model types. Average fault current magnitudes of 227A, 2421A and 1332A; and an average post fault current magnitudes of 41.4A, 103.4A and 24.0A can be seen for the start, middle and end of the line correspondingly. It is paramount to remember that all the aforementioned summary tables are constructed to indicate the longest circuit breaker clearance times; subsequently, some results contain high impedance circuits, whilst others have low impedance circuits.

Furthermore, it is clear Tables 5.1, 5.2 and 5.3 do not evenly represent the impact of the overall fault circuit impedance with respect to fault magnitude; however, when analysing Appendix B, C and D it is very clear that high impedance circuits have lower fault magnitude and low impedance circuits have higher fault magnitude; an average fault current of 6135A, 1966A and 4168A; and an average post circuit breaker clearance current magnitude of 215.3A, 133.3A and 112.2A can be seen for the start, middle and end of the line respectively. A detailed discussion of the implications of fault circuit impedance variation will be discussed in detail within the Fault Impedance Section of this chapter.

Table 5.2: Results Summary - Middle of Line - Table.

Model Type	Fault Impedance	Load (MW)	Max. Fault Duration (ms)	Inception Angle (°)	Fault Mag (A)	Post Fault Mag. (A)
DT	0	2000	96	60	4118	278.0
			96	90	5164	102.8
Mayr	1000	0	48	30	176	12.1
Cassie	1000	0	43	-60	224	20.6

When performing analysis of the summary tables (5.1, 5.2 and 5.3) it is important to remember that these results indicate the longest fault durations; and as such are the worst case scenario for each location and arc model type. The average fault duration from Appendix B, C and D is 56ms, 51ms and 58ms for the start, middle and end of the line respectively. In reality the average fault durations are more likely to occur; however, as protection schemes must be implemented that can handle all scenarios this study will focus on the worst case circuit breaker clearance times.

Table 5.3: Results Summary - End of Line - Table

Model Type	Fault Impedance	Load (MW)	Max. Fault Duration (ms)	Inception Angle (°)	Fault Mag (A)	Post Fault Mag. (A)
DT	1000	0	100	-30	403	33.2
Mayr	0	2000	57	90	3231	17.9
Cassie	1000	2000	38	-90	361	20.9

It is clear to see from Table 5.1, 5.2 and 5.3 that definite time arc modelling creates the longest fault durations of 99ms, 96ms and 100ms for the start, middle and end of the line respectively. However, as definite time modelling does not consider early fault extinction this study will utilise the Mayr and Cassie arc model times to determine realistic fault duration; subsequently, 46ms, 48ms and 57ms for the start, middle and end of the line respectively will be considered as the largest fault durations for each location.

5.2 Arc Model

Definite Time, Mayr and Cassie arc models were each used to simulate numerous fault and network conditions at all three (3) faulted line locations; thus meeting the requirements of objective E to utilise realistic arc models under various system faulted conditions. It is blatantly obvious that the definite time model will have the largest circuit breaker clearance time in all scenarios as it does not consider the early extinguish of the fault arc; whilst all model results will be discussed the primary focus of this section will be on the Mayr and Cassie arc models as they provide a much more realistic representation of the fault arc. Analysing the results in from Tables 5.1, 5.2, 5.3 it can be seen that the maximum fault duration utilising the Mayr arc model is consistently larger than that of the Cassie model.

Table 5.4 indicates the number of times that a longer fault duration has been recorded using identical system conditions varying only the arc model type; it is clear to see that the Mayr fault model consistently produces longer fault durations at all faulted locations. This reinforces the conclusions drawn from summary Tables 5.1, 5.2 and 5.3 that the longest fault duration will be modelled by the Mayr arc model.

Table 5.4: Mayr vs. Cassie Effect On Fault Duration

Location	Mayr Causes Longer Fault Duration	Cassie Causes Longer Fault Duration	Mayr/Cassie Causes Same Duration
Start	22	5	1
Middle	19	6	3
End	24	4	0

The number of times each fault model type produced a larger fault current magnitude at each location is show in Table 5.5. It is clear to see that definite time arc modelling consistently produces a larger fault current magnitudes. However, as previously indicated this study will focus on the Mayr and Cassie models as the definite time modelling does not simulate a change in impedance between the circuit breaker contacts as they part. This subsequently means that definite time modelling will have a lower fault circuit impedance that does not change for the entire fault duration; giving a larger fault current magnitude then is realistically experienced.

Table 5.5: Arc Model Effect On Fault Current Magnitude

Location	DT Causes Larger Fault Current	Mayr Causes Larger Fault Current	Cassie Causes Larger Fault Current
Start	16	4	8
Middle	13	5	10
End	23	4	1

When considering the Mayr and Cassie arc models only, Table 5.6 indicates the number of times each model produced a larger fault current magnitude at each location. It is interesting to note that the fault arc models appear to respond differently at each of the three faulted locations. The start of the line produces a relatively even distribution between the Mayr and Cassie model. The middle of the line shows the Cassie model producing larger fault magnitudes; conversely the end of the line shows the Mayr model producing larger fault magnitudes.

Table 5.6: Mayr vs. Cassie Effect On Fault Current Magnitude

Location	Mayr Causes Larger Fault Current	Cassie Causes Larger Fault Current
Start	15	13
Middle	9	19
End	19	9

Table 5.7 shows the number of times that each model produced a larger post fault magnitude at each location. Using the same justifications as the fault current magnitude it can be determined that the post fault current magnitude recorded by the definite time arc model will not experience accurate representation of the entire fault circuit impedance; hence, these results will not be used in determining the maximum post fault current magnitude.

Table 5.7: Arc Model Effect On Post Fault Current Magnitude

Location	DT Causes Larger Post Fault Current	Mayr Causes Post Larger Fault Current	Cassie Causes Larger Post Fault Current
Start	17	8	3
Middle	1	7	20
End	14	4	10

Comparing the number of times the Cassie or Mayr arc model created a larger post fault magnitude has been summarised in Table 5.8. It can be seen that the Mayr arc model produces large post fault current at the beginning of the line, whilst the Cassie arc model produces larger fault currents at the middle and end of the line.

Table 5.8: Mayr vs. Cassie Effect On Post Fault Current Magnitude

Location	Mayr Causes Larger Post Fault Current	Cassie Causes Larger Post Fault Current
Start	18	10
Middle	7	21
End	10	18

When performing simulations there were also noticeable arc characteristic differences between the Cassie and Mayr arc models. One such observational difference in the behaviour of the arc models was the abruptness of current chopping; Figure 5.1 is a good representation of the steepness that is achieved by the Cassie arc model when the fault arc is extinguished. Whilst this immediate change in current appears to be an accurate representation of current chopping it also causes simulation stability issues when the overall fault circuit impedance was low.

Figure 5.2 has the equivalent network configuration and system parameters to Figure 5.1 however it was simulated using the Mayr arc model; there appears to be very little or no current chopping upon the extinguish of the fault arc when using the Mayr model. This difference in current chopping was a common theme when comparing the behaviour of the two models. Extending upon this characterisation of arc models it can clearly be seen that the Cassie model produces larger and more abrupt current during the transient recovery period; this is also a common trend seen throughout all modelling results.

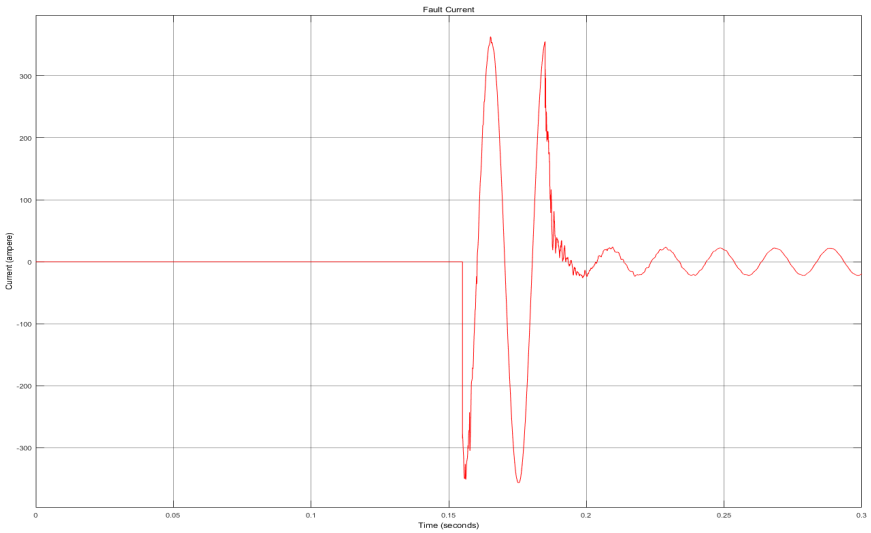

Figure 5.1: Cassie Model - Current Chopping

When analysing model behaviour during the simulation process it was noted the Cassie model responded well to high current simulations and poorly to low currents situations. Conversely, the Mayr model responded well to low current simulations and poorly to high current situations. Further investigation found that Gustavsson (2004) and Guardado & Maximox (2005) have reported similar model behaviour. When the aforementioned behaviour created model instability that prevented a small number of results from being obtained within this dissertations specific case study the relative and absolute tolerances were able to be marginally relaxed to achieve stability and the subsequent results.

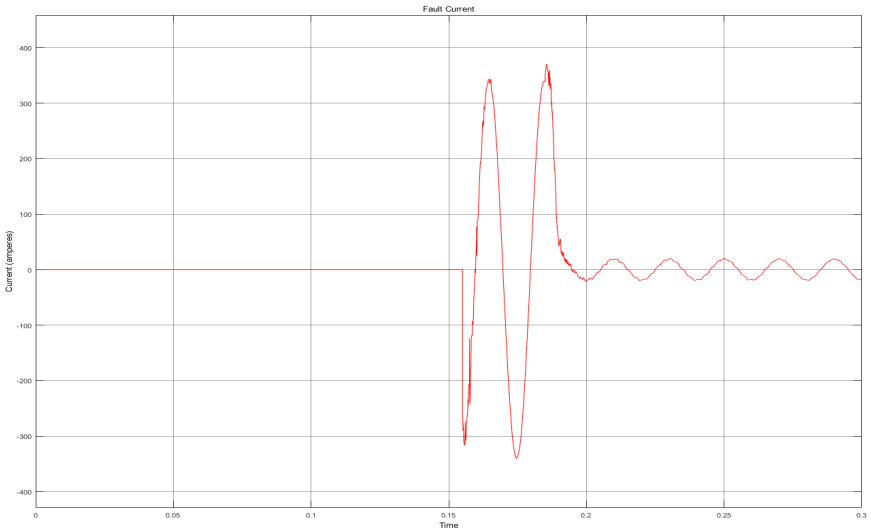

Figure 5.2: Mayr Model - Current Chopping

Throughout the vast majority of cases both the Cassie and Mayr model produce similar fault clearance times; for the purpose of this study the longer of the two time in each

scenario will be used for analysis to ensure the fault will have been cleared.

5.3 Fault Impedance

As with any electrical circuit when the series impedance is increased the resultant current will be decreased. When altering the fault circuit impedance to meet objective E this relationship was clear and obvious; all results contained within Appendix B, C and D show this fundamental relationship. It is also important to note the effect that the variation of impedance has on the fault duration. Table 5.9 is a summary showing which impedance had a longer fault duration for each scenario at each location. It is clear to see at the start of the line that 1000 Ω fault circuit impedance created a longer duration in the vast majority of cases. However for faults located at the middle or end of the line the longest durations were spread evenly for both low and high impedance faults.

Table 5.9: Impedance Effect On Time

Location	0 Ω Causes Longer Time	1000 Ω Causes Longer Time	0/1000 Ω Cause Identical Times
Start	7	32	3
Middle	21	19	2
End	18	20	4

Fault magnitudes contained within Appendix B, C and D having 0 Ω fault circuit impedance show an average magnitude of 12046A, 3698A, 7988A whilst fault circuits with 1000 Ω impedance show an average fault magnitude of 225A, 234A, 348A for the start, middle and end of the line accordingly. This produces an overall average fault magnitude of 6135A, 1966A and 4168A for the start, middle and end of the line respectively. As expected it is clear to see that the fault magnitude is highly dependent on the overall fault circuit impedance. It is not practicable to reproduce every variation of fault circuit impedance that could occur as there are no limitation to the combination of impedances available; however, it is clear from the results obtained that an impedance between the 0 Ω and 1000 Ω must follow Ohms law and produce an according proportional magnitude.

Figures 5.3 and 5.4 are a good example of the reduction in current and increase in duration. Both simulations were performed under identical fault conditions with the only variation

being the fault circuit impedance; Figure 5.3 has a fault impedance of 0 Ω and Figure 5.4 has a fault impedance of 1000 Ω.

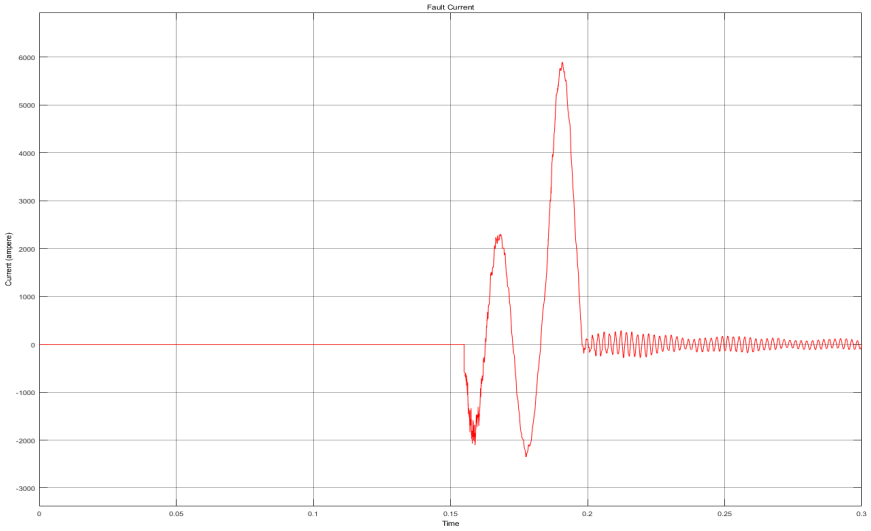

Figure 5.3: Mayr Model - 0 Ω Impedance

The faulted current magnitude with 0Ω impedance is 5866A and has a duration of 43ms, whilst the faulted magnitude with 1000Ω impedance is 217A with a duration of 52ms. The high impedance simulation has approximately 27 times less current and lasts 9ms longer. As predicted the 1000Ω impedance greatly reduced the magnitude of the faulted current, which is explained by basic electrical theory; however, it was also predicted that the fault duration would be longer for the higher fault currents, this did not specifically hold true in all cases.

It has also been consistently observed that low fault circuit impedances experience high frequency oscillation throughout both the transient recovery voltage period and the recovery voltage period. This behaviour is not seen for faults with high circuit impedance; the transient recovery voltage will display high frequency oscillation, however, this will transform into 50Hz oscillation when the transition into the recovery voltage period occurs.

This behaviour is intuitive and can be explained by fundamental theory; when a 0Ω impedance fault occurs it is essentially shorting the faulted phase directly to earth. This short to ground effectively reduces the distance for the remaining two phases to earth; hence, the phase to ground capacitive effect is now the spacing between the energised phases and faulted phase rather than the height of the conductor to earth. It is obvious that a scaled down version of the aforementioned effect will also be seen with the 1000Ω

impedance fault; however, as the impedance is so high the coupling behaviour seen will be similar to that of an open and unearthed phase.

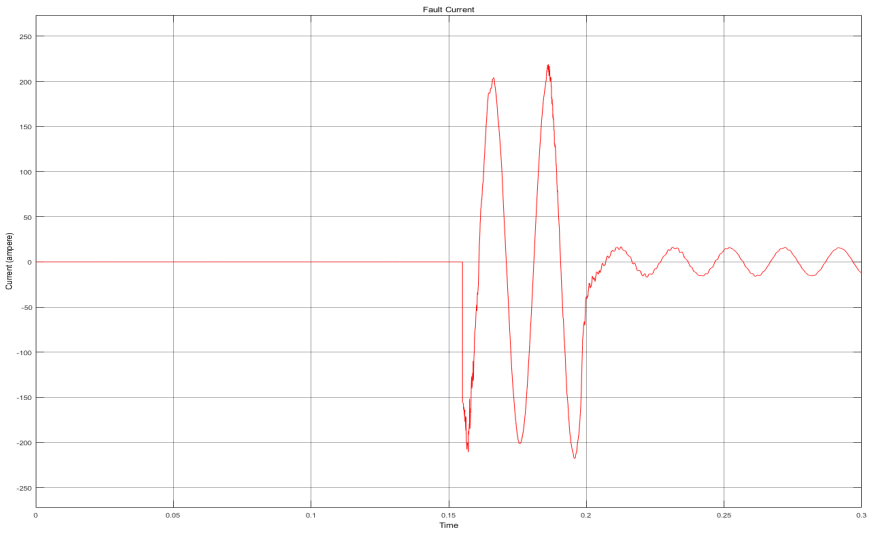

Figure 5.4: Mayr Model - 1000 Ω Impedance

Adding to the above fault characteristics it was also noted that the additional fault circuit impedance adds to the stability of the entire simulated model. This added stability is due to the softening of current chopping that is experienced when a fault is extinguished. It is widely known that Mathworks Simulink Simscape Power Systems often has issues simulating numerical functions that are considered stiff. Various ODE (ordinary differential equation) solvers can be chosen to aid in the modelling of very stiff functions, however in some instances additional fault circuit impedance was required to successfully simulate the fault. Cassie models with 0Ω fault impedance at the start, middle and end were all initially unstable; hence, an additional 10Ω was added to the series fault circuit impedance of these systems in order to maintain simulation stability.

5.4 System Load

To enable the successful completion of objective E each variation of system conditions and network configuration were simulated with 0MW load, then repeated with 2000MW load. It was predicted that a larger load would produce longer fault durations and higher post fault currents for all system conditions and fault locations. Table 5.10 summarises the results found within Appendix B, C and D showing the number of times a longer fault duration is seen for identical system conditions varying only the load. It can be

seen that the vast majority of faults at the start of the line have a longer fault duration when subject to high load, however, faults in the middle of the line have an even balance between high and low loading. Converse to initial predictions fault durations at the end of the line have a substantial number of fault durations that are longer for low system loading.

Table 5.10: System Load Effect On Time

Location	0MW Causes Longer Time	2000MW Causes Longer Time	0/2000MW Cause Identical Times
Start	20	13	9
Middle	16	14	12
End	9	25	8

Table 5.11 shows the number of occasions when the variation of load produced a higher fault current magnitude. It was initially predicted that the higher network load would produce larger fault currents; however, Table 5.11 shows that larger fault currents are seen more often when 0MW of load is being supplied at each of the faulted locations.

Table 5.11: System Load Effect On Fault Current

Location	0MW Causes Larger Arc Current	2000MW Causes Larger Arc Current
Start	31	11
Middle	23	19
End	34	8

The number of occasions when the variation of load produced a higher post fault current is shown within Table 5.12. It is abundantly clear that the start and the middle of the line produce larger post fault currents when the load is increased; however, a fault at the end of the line has almost equal distribution between 0MW and 2000MW.

Table 5.12: Post Fault Current

Location	0MW Causes Higher Post Fault Current	2000MW Causes Higher Post Fault Current
Start	31	11
Middle	31	11
End	20	22

Figure 5.5 is a fault current recorded when 0MW is supplied to the load; while Figure 5.6 is a fault current recorded at 2000MW load under identical network conditions and parameters. Although the increase of load did not necessarily mean an large increase in fault duration and post fault current magnitude in all cases two major behavioural trends were observed. Figure 5.5 and Figure 5.6 are good indications of the trends seen throughout all variations and clearly indicate the simulation at higher load is subject harsh current chopping at fault extinguish and high frequency oscillations in the recovery period; whereas the lower load has a smoother transition at fault extinguish and nominal frequency oscillation throughout the recovery period.

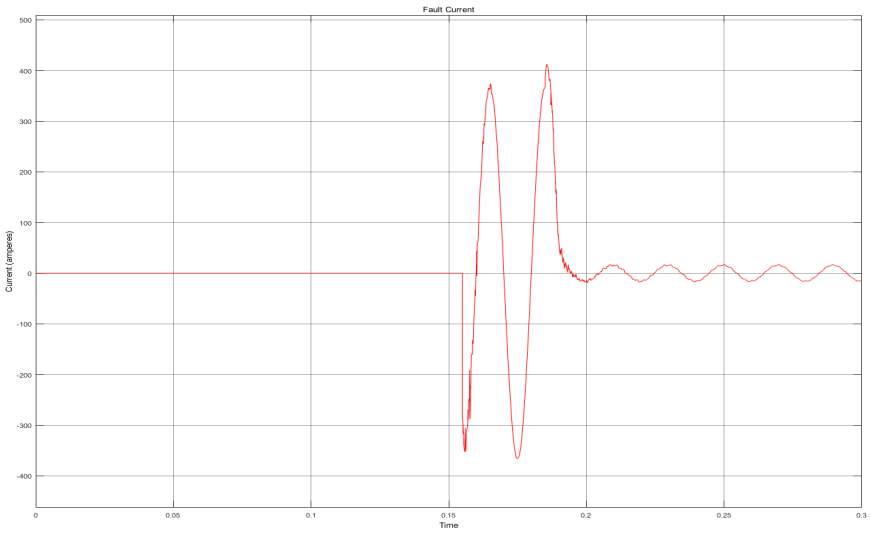

Figure 5.5: Mayr Model - 0MW Load

It is clear to see that when comparing Figure 5.5 and 5.6 the latter has an additional half cycle where the fault current continues to oscillate and the former peters out when approaching zero. The time for the first zero current crossing after the primary arc of the fault is extinguished appears to be similar in both cases. It can be seen that the no load fault waveform transitions into the current created by the electromagnetic and electrostatic induction before it crosses zero, whereas the fault with load is subject to

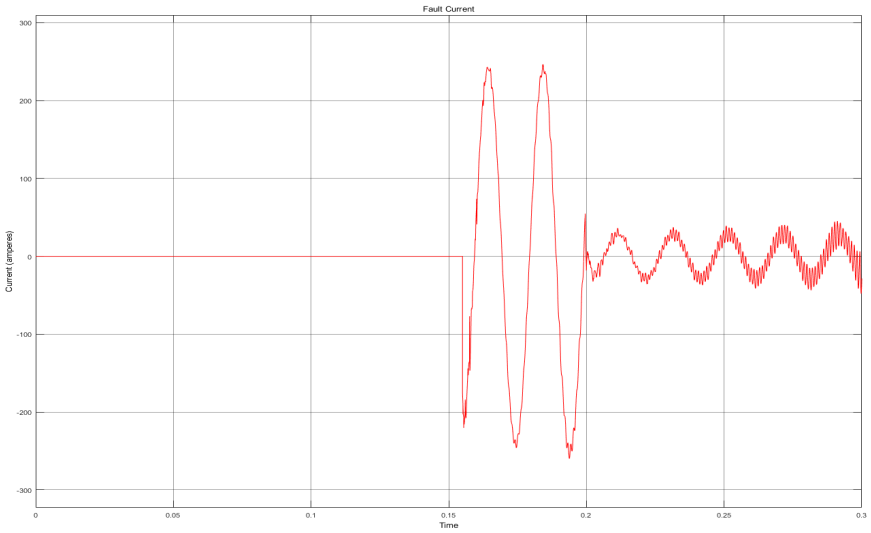

Figure 5.6: Mayr Model - 2000MW Load

current chopping and subsequently stops abruptly. It is obvious that the waveform of the higher load will have a much harsher impact on the network stability and primary plant; however, when considering objective F the purpose of this study is to focus on the overall fault clearance time from a protection perspective to enable minimum circuit breaker failure time to be established. Subsequently, when analysing faults with the same overall duration they will be considered similar regardless of the degree to which the fault current peters out or is subject to current chopping.

5.5 Inception Angle

As detailed within the methodology chapter the inception angle was varied between -90° and 90° in steps of 30° to contribute towards objective E. It is summarised that the vast number of interconnected network components make trending the outcomes of inception angle variation impossible on an entire line scale. However, it is clear in each individual system configuration shown within Appendix B, C and D that the variation of inception angle causes numerous responses in the resultant fault current. The inception angle is deemed the electrical angle at which the fault occurs at the faulted location, the instant before the fault occurs; hence, achieving the same inception angle at different locations along a line will require various changes to the short circuit sources. As the short circuit sources drastically alter the system characteristics it is clear to see why the same inception angle at a different location will not follow a trend.

Although an overall inception angle trend could not be determined a number of characteristics were identified. Figure 5.7 and 5.8 both clearly show a DC offset in the faulted current waveform; however one DC offset is positive then angled down, while the other DC offset is negative then angled up. This behaviour was particularly prominent when utilising definite time models as the fault duration was much longer showing many more cycles; hence, the DC offset was much easier to establish. When utilising Mayr and Cassie models it was difficult to determine if the DC offset was applicable; however, when the Mayr and Cassie fault duration was extend to produce additional faulted cycles it was clear that similar behaviour can be seen. Subsequently, it can be said that altering the inception angle will vary the DC offset in the resultant fault current throughout all modelled results.

When analysing why this behaviour occurs it is important to consider that the inception angle represents the electrical angle at the instant before the fault; this leads to the understanding that the inception angle will alter the overall shape and behaviour of the faulted waveform. Figure 5.7 initially shows a largely positive fault current which is angled downward as the fault continue, giving the overall wave a positive DC offset.

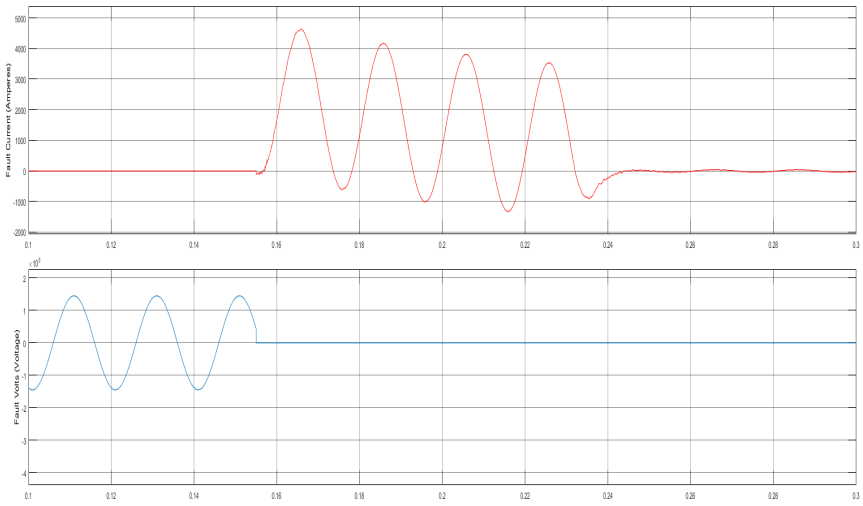

Figure 5.7: Positive DC Offset

Figure 5.8 initially shows a largely negative fault current which is angled upward as the fault continues, giving the overall wave a negative DC offset. This trend can consistently be seen throughout all the results as the inception angle is varied.

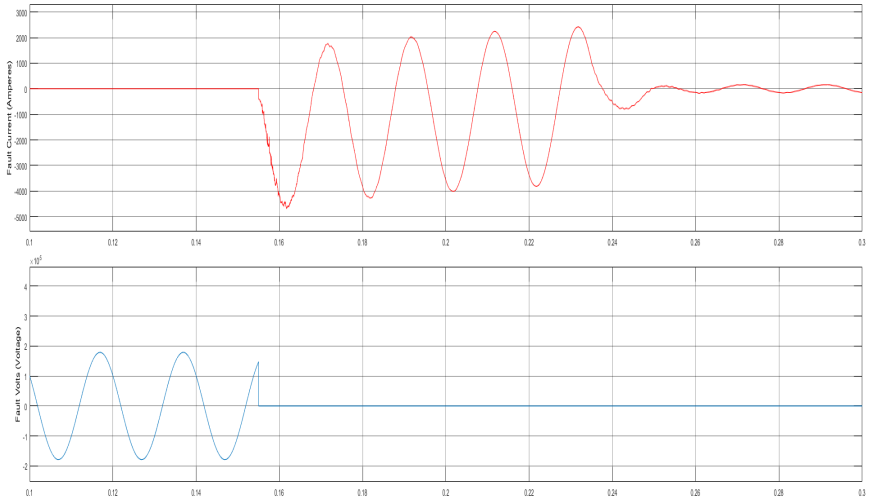

Figure 5.8: Negative DC Offset

When considering results in Appendix B, C and D it is clear to see that the inception angle has an effect not only on the fault duration but also the fault current magnitude.

5.6 Application of Results

The following section will discuss the application of the results obtained throughout this study; the aim to meet objective F by determining a realistic minimum circuit breaker failure time. It is clear that the longer of the Mayr and Cassie times for each location will be utilised to ensure fault clearance in each scenario. Tables 5.1, 5.2 and 5.3 show that the maximum fault duration is 46ms, 48ms and 57ms for the start, middle, and end of the line respectively. It is important to remember that these aforementioned times are the entire fault duration; this becomes paramount when calculating circuit breaker failure timing as 30ms has been allowed for the primary protection element to detect and operate. Circuit breaker failure times are calculated after this initial detection. Hence, the circuit breaker clearing times of 16ms, 18ms and 27ms for the start, middle, and end of the line respectively will be used to determine the circuit breaker failure times.

As current protection systems do not use fault location within a single protected scheme to distinguish circuit breaker failure times the greatest of the three location times will be used as the circuit breaker clearance time for the entire line. The greatest time for the three (3) locations is 27ms and subsequently this time will be used for further analysis.

Whilst the longest circuit breaker clearance time has been determined above it is paramount to remember that unique protection devices will require individual analysis to produce the most effective circuit breaker failure time. Firstly, a generic circuit breaker failure time will be determined; this will be used for comparison with specific circuit breaker failure times. Secondly, two (2) relay specific times will be determined using the recommended parameters of the specific line protection relays chosen. The two (2) specific circuit breaker failure times will be for a General Electric L90 and Schneider MiCom P546 as these are prominent throughout the Australian transmission network.

Atienza, E and Moxley, R (2011) stipulate that when implementing a traditional circuit breaker failure schemes with standard protection elements and standard output contacts the minimum circuit breaker failure time can be found using the following: Generic CBF Time = Max CB Clearing Time + Open Phase Detection + Security Margin + Maximum Trip Output Contact Time - Minimum CBF Initiate Time. Using the reccomended values given by Atienza, E and Moxley, R (2011) and the CB clearance time determined within this study equation 5.1 can be formed;

$$Generic\,CBF\,Time\,(ms) \;=\; 27ms + 30ms + 40ms + 7.2ms - 10ms \;=\; 94.2ms \quad (5.1)$$

GE Industrial Systems (2009) state that the minimum circuit breaker failure time for a GE L90 (General Electric L90) should consist of the following: L90 CBF Time = Breaker Interrupting Time + Margin + Breaker Failure Current Detector + Braker Failure Output Relay Pickup. Using the reccomended values given by GE Industrial Systems (2009) and the CB clearance time determined within this study equation 5.2 can be formed;

$$L90\;CBF\;Time\;(ms) \;=\; 27ms \;+\; 40ms \;+\; 20ms \;+\; 20ms \;=\; 107ms \quad (5.2)$$

Schneider (2012) state that the minimum circuit breaker failure time for a Schneider MiCom P546 should consist of the following: P546 CBF Time = CB interrupting time + undercurrent element operating time (max) + safety margin. Using the reccomended values given by Schneider (2012) and the CB clearance time determined within this study equation 5.3 can be formed;

$$P546\;CBF\;Time\;(ms) \;=\; 27ms \;+\; 12ms \;+\; 50ms \;=\; 89ms \quad (5.3)$$

The above paragraphs and calculations make it abundantly clear that when the same circuit breaker clearance time is utilised in different protection devices an individual cal-

culation and subsequent circuit breaker failure time will be required. This is paramount when considering that transmission authorities utilise duplicate X and Y line protection schemes employing different relay manufacturers for each; the three (3) circuit breaker failure times, 94.2ms, 107ms and 89ms for differing protection devices with the same circuit breaker clearance time are a good indication of the variation that can be seen between devices.

5.7 Chapter Summary

The results chapter contains various summaries of the tabulated results contained within Appendix B, C and D; behavioural and characteristic trends seen throughout the simulations are also discussed in great detail. Some major aspects discussed were the abruptness of current chopping and transient recovery period behaviours when the arc model is varied, effects on fault current and post fault current magnitudes when fault circuit impedance varied and the DC offset caused by the alteration of inception angle. This section continued further; applying the results obtained through the study three (3) circuit breaker failure times were determined for the specific case study; GE L90 as 107ms, MiCom P546 as 89ms and a generically applicable CBF time as 94.2ms.

Chapter 6

Conclusions and Further Work

6.1 Conclusions

The main objective of this dissertation was to establish a technique to determine the maximum fault duration on a transmission network that utilises single pole tripping. This aim extended to the utilisation of this time to determine a minimum circuit breaker failure time for the aforementioned network. In achieving this main project objective a number of smaller sub-objectives were created; simulation of a transmission network, variation of load flow, inception angle alteration, high and low fault circuit impedance and multiple fault model types.

It was found that the longest fault duration of 100ms was produced using definite time modelling; however, definite time modelling has two (2) major flaws: firstly it does not consider the early extinguish of a faulted arc, secondly, as the contacts open instantaneously after a specific period of time the variation of impedance as contact part is not seen. Subsequently it was determined that the definite time fault modelling did not produce a realistic representation of fault current magnitude or fault duration.

Mayr and Cassie arc modelling were then utilised to provide a realistic representation of the fault current magnitude and fault duration; the longest overall fault duration was produced by the Mayr arc model and was determined to be 57ms. Noting this time is the entire fault duration a CB clearing time of 27ms was calculated.

Finally it was shown that effective circuit breaker failure times are highly dependent on

not only the circuit breaker clearance time, but also the protection device used; hence, each circuit breaker failure time should be calculated specifically for each circuit breaker and protection device. A generic circuit breaker failure time of 94.2ms was determined followed by two (2) device specific times of 107ms and 89ms for the GE L90 CBF and Schneider MiCom P546 CBF respectively.

6.2 Further Work

All the items outlined in the project specification were successfully addressed; however, there are a number of items that presented themselves during the course of this project that could be further work for either other students or the author.

1) The use of a hybrid Cassie-Mayr arc model would greatly increase the accuracy of results and the stability of the simulations. Investigation has established that the Cassie arc model performs better when modelling large currents and can become unstable at low currents; while the Mayr arc model performs well at low currents and poorly at high currents.

2) The use of other additional/different models within the same transmission network; such models could include linear variants such as the Kema arc model, or advanced models such as the Magneto-Hydrodynamic model which utilises Navier-Stokes equations for energy coupled with Maxwell equations.

3) Investigate the possibility of fault location based CBF times within a single protection scheme. The possibility of using distance protection elements to determine the faulted location; subsequently utilising individual CBF times specific to a location along the line.

References

ABB (2014), 'Live Tank Circuit Breaker's Buyers Guide', https://library.e.abb.com/public/433e1e613e67d06ec1257d0400307817/Buyers%20Guide%20HV%20Live%20Tank%20Circuit%20Breakers%20Ed%206en.pdf.

AEMO (2012), 'Short-circuit levels for victorian electricity transmission: 2013-2017', https://www.aemo.com.au/.../ShortCircuitLevels_VictorianElectricityTransmission_2013_2017.ashx.

AEMO (2013), 'Victorian annual planning report - electricity transmission network planning for victoria', file:///C:/Users/Brad/Downloads/Victorian_Annual_Planning_Report_2013_v2.pdf.

Ahmethodzic, A., Kapetanovic, M., Sokolija, K., Smeets, R. P. P. & Kertesz, V. (2011), 'Linking a physical arc model with a black box arc model and verification', *IEEE Transactions on Dielectrics and Electrical Insulation* **18**(4), 1029–1037.

Alstom (2010), 'Gl314(x) to Gl318(x) Live tank circuit breakers from 245kv to 800kv', https://www.gegridsolutions.com/alstomenergy/grid/Global/Grid/Resources/Circuit%20Breakers/Documents/GL314(X)%20to%20GL318(X)%20Live%20tank%20circuit%20breakers%20from%20245%20kV%20to%20800%20kV%20Brochure%20GB.fr-FR-epslanguage=fr-FR.pdf.

Andrade,V and Sorrentino, E (2010), 'Typical expected values of the fault resistance in power systems', http://webspace.ulbsibiu.ro/maria.vintan/html/Citare_2010.pdf.

Atienza, E and Moxley, R (2011), 'Improving breaker Failure Clearing Times', https://cdn.selinc.com//assets/Literature/Publications/Technical%20Papers/6384_ImprovingBreaker_EA_20090917_Web.pdf?v=20151124-140452.

Bizjak, G., Zunko, P. & Povh, D. (1995), 'Circuit breaker model for digital simulation based on Mayr's and Cassie's differential arc equations', *IEEE Transactions on Power Delivery* **10**(3), 1310–1315.

Costa, F., Souza, B. & Brito, N. (2012), 'Effects of the fault inception angle in fault-induced transients.', *IET Generation, Transmission & Distribution* **6**(5), 463–471.

GE Group (2002), 'High Voltage Transmission Line Protection with Single Pole Tripping and Reclosing', `http://store.gedigitalenergy.com/faq/documents/ALPS/GET-6555.pdf`.

GE Industrial Systems (2009), 'L90 Line Differential Relay', `https://gegridsolutions.com/products/manuals/l90/l90man-f4.pdf`.

Goday, E. and Celaya, A (2012), 'Tutorial on Single-Pole Tripping and Reclosing', `https://cdn.selinc.com//assets/Literature/Publications/Technical%20Papers/6579_TutorialSingle_NF_20120912_Web.pdf?v=20151125-094230`.

Guardado, J. & Maximox, G. (2005), 'An Improved Arc Model Before Current Zero Based on the Combined Mayr and Cassie Arc Models', *IEEE Transactions on Power Delivery* **20**(1), 138–143.

Gustavsson, N. (2004), 'Evaluation and Simulation of Black-box Arc Models for High Voltage Circuit-breakers', `http://www.control.isy.liu.se/student/exjobb/xfiles/3492.pdf`.

Horton, R., Halpin, M. & Wallace, K. (2006), 'Induced Voltage in Parallel Transmission Lines Caused by Electric Field Induction'.

Jannati, M., Vahidi, B., Hosseinian, S. H. & Ahadi, S. M. (2011), 'A novel approach to adaptive single phase auto-reclosing scheme for Ehv transmission lines', *International Journal of Electrical Power and Energy Systems* **33**(3), 639–646.

Jeerings, D. I. & Linders, J. R. (1989), 'Ground resistance-revisited', *IEEE Transactions on Power Delivery* **4**(2), 949–956.

Mathworks(a) (2016), 'Cassie and Mayr Arc Models for a Circuit Breaker', `http://au.mathworks.com/help/physmod/sps/examples/cassie-and-mayr-arc-models-for-a-circuit-breaker.html`.

Mathworks(b) (2016), 'Three Phase Pi Section Line', `http://au.mathworks.com/help/physmod/sps/powersys/ref/threephasepisectionline.html`.

Mathworks(c) (2016), 'Distributed Parameter Line', http://au.mathworks.com/help/physmod/sps/powersys/ref/distributedparameterline.html;jsessionid=42ffa45cd2cc54cc71fad1aee0b4?refresh=true.

Mathworks(c) (n.d.), 'Three Phase Source', http://au.mathworks.com/help/physmod/sps/powersys/ref/threephasesource.html?searchHighlight=three%20phase%20source.

Ngamsanroaj, S. & Watson, N. (2014), '500kv Single Phase Reclosing Evaluation Using Simplified Arc Model', *International Journal of Emerging Technology and Advanced Engineering* **4**(6).

NTT Technical (2007), 'Calculation Method to Estimate Electrostatic and Electromagnetic Induction in the Design of Telecommunication Facilities', *NTT Technical Review* **5**(8).

Oh, Y. and Song, K. (2015), 'The calculation of arc conductance in sf6-n2 mixture gas circuit breaker', http://ieeexplore.ieee.org/xpl/login.jsp?tp=&arnumber=7368419&url=http%3A%2F%2Fieeexplore.ieee.org%2Fxpls%2Fabs_all.jsp%3Farnumber%3D7368419.

Pinto, A. J. G., Costa, E. C. M., Kurokawa, S., Monteiro, J. H. A., de Franco, J. L. & Pissolato, J. (2014), 'Analysis of the electrical characteristics and surge protection of Ehv transmission lines supported by tall towers', *International Journal of Electrical Power & Energy Systems* **57**, 358–365.

Schavemaker, P. H. & van der Slui, L. (2000), 'An improved Mayr-type arc model based on current-zero measurements', *IEEE Transactions on Power Delivery* **15**(2), 580–584.

Schneider (2012), 'Micom P54x Technical Manual', http://download.schneider-electric.com/files?p_Reference=P54x_EN_M_H53__V30&p_EnDocType=User%20guide&p_File_Id=315496381&p_File_Name=P54x_EN_M_H53__V30_J.pdf.

Siemens (2008), 'Operating instructions circuit-breaker 3ap3 fi', .

Smeets, R. R. & Kertsz, V. (2000), 'Evaluation of High Voltage Circuit Breaker Performance with a Validated Arc Model', *IEE Proceedings - Generation, Transmission and Distribution* **147**(2), 148–151.

Appendix A

Project Specification

The following appendix will include the agreed final project specification.

For:	**Bradley Wentworth**
Topic:	Circuit Breaker Simulated Operation & Behaviour Under Faulted Power System Conditions
Major:	Power Engineering
Supervisors:	Tony Ahfock
Project Aim:	To be able to determine the realistic clearance time for a high voltage circuit breaker from fault initiation to fault extinguish during faulted power system conditions under various network configurations/conditions. Apply these findings to a three phase network where minimal clearance and circuit breaker failure times are required to ensure network stability.

Program: Issue B, 12th May 2016

- Examine existing information on EHV (Extra High Voltage) CB (Circuit Breaker) fault modelling/data and review for applicability.
  - Determine if existing EHV CB simulation models exist and are available.
  - Assess applicability of existing EHV CB models for single phase fault application on a three phase network.
  - Assess EHV CB arcing model applicability for a phase to ground fault.
- Determine the characteristics of three (3) phase (single pole operated) EHV CB.
  - Establish how an EHV CB will behave under a single phase fault conditions.
  - Determine if this behaviour can adequately be modelled using methods determined in dot point one (1).
- Utilise EHV CB models to simulate a power network that can achieve the single pole tripping characteristics defined in dot point two (2)
- Determine a realistic fault characteristic for a single phase fault in a three phase power system.
  - Determine factors that influence non-instantaneous arc-extinction.
  - Establish a definite maximum fault time.

  - Utilise a realistic circuit breaker arcing model to determine realistic fault time.

- Utilise a realistic arc model under various system fault conditions.
  - Varying fault location throughout the network
  - Varying inception angle of the fault
  - Varying the loading conditions the network is subjected to at the time of fault.
  - Varying the behaviour of the phase to ground fault to assess time implications.
- Analyse fault clearance times to determine a realistic circuit breaker failure time
  - Compare various fault times and conditions to determine a maximum fault time and subsequent minimum EHV CB failure time.

As time and resources permit:

- Utilise and verify a second realistic arc model under various system and faulted conditions.
  - Varying fault location throughout the network
  - Varying inception angle of the fault
  - Varying the loading conditions the network is subjected to at the time of fault.
  - Varying the behaviour of the phase to ground fault to assess time implications.
- Analyse fault clearance times of the second arc model to determine a realistic circuit breaker failure time
  - Compare various fault times and conditions to determine a maximum fault time and subsequent minimum EHV CB failure time.
- Compare results obtained from different arc models.

Appendix B

Start of Line Results

The following appendix will include the DT, Mayr and Cassie tabulated results for the start of the line fault.

Table B.1: Results - DT - Start of Line - Table.

Fault Imp. (Ω)	Load (MW)	Inception Angle (°)	Fault Init. (ms)	Fault Ext. (ms)	Fault Mag. (A)	Post Fault Mag. (A)
0	0	-90	155	242	12970	454.2
		-60	155	243	21930	341.5
		-30	155	245	27720	378.8
		0	155	245	28300	553.9
		30	155	246	25680	722.3
		60	155	248	23590	991.9
		90	155	242	12970	442.5
0	2000	-90	155	242	12860	413.1
		-60	155	244	19090	372.2
		-30	155	244	25200	377.7
		0	155	245	28760	569.8
		30	155	246	26520	650.9
		60	155	248	23640	917.9
		90	155	248	40200	1253.0
1000	0	-90	155	251	160.8	38.8
		-60	155	252	245.1	26.5
		-30	155	253	273.7	31.5
		0	155	254	236.0	49.1
		30	155	245	214.6	61.3
		60	155	247	193.4	85.3
		90	155	251	161.3	38.7
1000	2000	-90	155	251	158.7	34.5
		-60	155	244	223.8	29.9
		-30	155	245	263.5	31.9
		0	155	245	260.9	47.6
		30	155	245	219.8	55.6
		60	155	246	188.4	76.3
		90	155	247	297.5	106.0

Table B.2: Results - Mayr - Start of Line - Table.

Fault Imp. (Ω)	Load (MW)	Inception Angle (°)	Fault Init. (ms)	Fault Ext. (ms)	Fault Mag. (A)	Post Fault Mag. (A)
0	0	-90	155	186	21460	537.2
		-60	155	199	17102	244.0
		-30	155	198	99937	190.3
		0	155	195	10701	321.4
		30	155	195	12384	299.6
		60	155	195	8134	202.2
		90	155	186	23260	482.0
0	2000	-90	155	196	4183	278.2
		-60	155	196	1702	180.1
		-30	155	195	2453	168.5
		0	155	192	7837	205.7
		30	155	194	9088	270.1
		60	155	196	9421	335.3
		90	155	196	4315	332.2
1000	0	-90	155	193	253.4	49.1
		-60	155	192	147.7	43.9
		-30	155	201	217.1	40.7
		0	155	197	187.4	40.1
		30	155	199	193.6	44.8
		60	155	197	178.9	47.1
		90	155	192	259.7	50.9
1000	2000	-90	155	198	175.8	47.7
		-60	155	198	185.6	53.0
		-30	155	198	186.8	56.7
		0	155	191	185.6	33.4
		30	155	200	182.3	37.6
		60	155	198	172.8	44.1
		90	155	198	176.4	48.9

Table B.3: Results - Cassie - Start of Line - Table.

Fault Imp. (Ω)	Load (MW)	Inception Angle (°)	Fault Init. (ms)	Fault Ext. (ms)	Fault Mag. (A)	Post Fault Mag. (A)
10	0	-90	155	190	2687	334.7
		-60	155	186	2165	322.0
		-30	155	191	2416	407.4
		0	155	191	2842	418.8
		30	155	191	2679	356.1
		60	155	192	2538	326.0
		90	155	190	2699	330.0
10	2000	-90	155	191	2480	221.5
		-60	155	189	2446	234.4
		-30	155	187	2087	133.3
		0	155	186	2347	??
		30	155	190	2332	261.4
		60	155	190	2304	326.9
		90	155	186	2489	??
1000	0	-90	155	197	251.7	45.5
		-60	155	197	205.0	43.5
		-30	155	191	383.6	49.2
		0	155	192	337.8	43.7
		30	155	195	311.8	38.1
		60	155	196	275.4	44.2
		90	155	197	255.1	46.0
1000	2000	-90	155	197	238.4	42.3
		-60	155	198	229.2	34.3
		-30	155	190	193.9	35.6
		0	155	188	216.5	47.9
		30	155	194	275.5	37.8
		60	155	196	239.0	26.3
		90	155	197	241.3	43.6

Appendix C

Middle of Line Results

The following appendix will include the DT, Mayr and Cassie tabulated results for the middle of the line fault.

Table C.1: Results - DT - Middle of Line - Table.

Fault Imp. (Ω)	Load (MW)	Inception Angle (°)	Fault Init. (ms)	Fault Ext. (ms)	Fault Mag. (A)	Post Fault Mag. (A)
0	0	-90	155	250	4595	162.7
		-60	155	239	4874	170.5
		-30	155	248	4663	184.4
		0	155	244	5300	171.5
		30	155	243	7050	109.4
		60	155	245	4631	42.11
		90	155	250	4630	158.8
0	2000	-90	155	250	5157	100.9
		-60	155	241	4649	116.6
		-30	155	240	5202	118.6
		0	155	244	4948	153.1
		30	155	242	4565	119.5
		60	155	251	4118	278.0
		90	155	251	5164	102.8
1000	0	-90	155	245	177.4	14.2
		-60	155	245	214.1	15.3
		-30	155	245	234.3	16.0
		0	155	241	211.6	13.6
		30	155	239	233.6	10.2
		60	155	239	145.7	4.6
		90	155	245	176.7	14.3
1000	2000	-90	155	242	258.4	9.3
		-60	155	243	311.1	9.7
		-30	155	241	328.2	10.2
		0	155	238	201.6	15.3
		30	155	240	256.6	12.2
		60	155	240	203.2	28.2
		90	155	241	291.5	12.1

Table C.2: Results - Mayr - Middle of Line - Table.

Fault Imp. (Ω)	Load (MW)	Inception Angle (°)	Fault Init. (ms)	Fault Ext. (ms)	Fault Mag. (A)	Post Fault Mag. (A)
0	0	-90	155	199	2999	82.3
		-60	155	202	2813	204.4
		-30	155	198	6615	238.0
		0	155	198	4970	463.6
		30	155	198	4686	325.9
		60	155	192	1423	151.5
		90	155	199	3075	169.1
0	2000	-90	155	191	835.2	173.4
		-60	155	197	885.0	107.3
		-30	155	198	6875	251.0
		0	155	198	5161	432.9
		30	155	199	4615	272.7
		60	155	194	1358	142.5
		90	155	191	844.6	168.6
1000	0	-90	155	191	129.4	9.7
		-60	155	196	70.84	5.0
		-30	155	190	280.3	22.8
		0	155	196	214.9	20.0
		30	155	203	176.0	12.1
		60	155	195	77.21	6.3
		90	155	191	131.6	10.7
1000	2000	-90	155	195	100.1	4.8
		-60	155	193	93.9	2.4
		-30	155	191	293.5	21.3
		0	155	196	228.2	16.4
		30	155	202	171.6	12.4
		60	155	194	75.9	6.8
		90	155	195	91.9	4.6

Table C.3: Results - Cassie - Middle of Line - Table.

Fault Imp. (Ω)	Load (MW)	Inception Angle (°)	Fault Init. (ms)	Fault Ext. (ms)	Fault Mag. (A)	Post Fault Mag. (A)
10	0	-90	155	190	3489	512.6
		-60	155	187	2080	334.9
		-30	155	191	2103	533.3
		0	155	190	2707	214.4
		30	155	191	3060	313.4
		60	155	191	3489	464.8
		90	155	190	3494	532.4
10	2000	-90	155	190	2058	500.0
		-60	155	187	2429	361.0
		-30	155	191	2453	328.0
		0	155	191	2330	213.6
		30	155	191	2428	224.2
		60	155	191	3059	348.0
		90	155	191	3428	499.6
1000	0	-90	155	195	329.0	25.1
		-60	155	198	224.0	20.6
		-30	155	197	237.7	19.0
		0	155	196	262.5	21.4
		30	155	196	282.8	25.6
		60	155	187	324.4	26.5
		90	155	195	331.3	27.3
1000	2000	-90	155	190	217.5	22.8
		-60	155	190	246.1	22.1
		-30	155	189	242.6	18.0
		0	155	196	239.2	12.5
		30	155	196	861.2	17.5
		60	155	196	285.3	22.1
		90	155	196	317.8	24.4

Appendix D

End of Line Results

The following appendix will include the DT, Mayr and Cassie tabulated results for the end of the line fault.

Table D.1: Results - DT - End of Line - Table.

Fault Imp. (Ω)	Load (MW)	Inception Angle (°)	Fault Init. (ms)	Fault Ext. (ms)	Fault Mag. (A)	Post Fault Mag. (A)
0	0	-90	155	247	19410	256.6
		-60	155	247	18660	318.4
		-30	155	247	18600	320.9
		0	155	247	18620	252.8
		30	155	247	19280	257.9
		60	155	247	19380	259.0
		90	155	247	19450	258.5
0	2000	-90	155	247	16970	226.0
		-60	155	248	17190	168.2
		-30	155	253	12740	270.5
		0	155	248	16580	385.3
		30	155	248	16480	299.7
		60	155	248	16810	259.1
		90	155	248	16910	227.7
1000	0	-90	155	252	403.0	25.2
		-60	155	255	401.4	32.9
		-30	155	254	403.2	33.2
		0	155	252	401.0	24.8
		30	155	252	402.8	25.6
		60	155	252	403.0	26.0
		90	155	252	403.1	25.7
1000	2000	-90	155	253	365.7	22.9
		-60	155	253	353.9	17.7
		-30	155	240	236.6	56.8
		0	155	254	385.2	39.3
		30	155	254	375.7	30.1
		60	155	254	370.6	25.6
		90	155	253	365.7	23.2

Table D.2: Results - Mayr - End of Line - Table.

Fault Imp. (Ω)	Load (MW)	Inception Angle (°)	Fault Init. (ms)	Fault Ext. (ms)	Fault Mag. (A)	Post Fault Mag. (A)
0	0	-90	155	192	3671	6.0
		-60	155	210	3445	21.3
		-30	155	191	2963	21.5
		0	155	191	3193	20.4
		30	155	211	3992	19.6
		60	155	191	3532	24.4
		90	155	203	3670	32.0
0	2000	-90	155	191	3561	12.8
		-60	155	194	2548	9.2
		-30	155	191	469	6.2
		0	155	190	1789	19.8
		30	155	211	3497	20.7
		60	155	211	3386	20.9
		90	155	212	3231	17.9
1000	0	-90	155	190	402.7	23.7
		-60	155	199	360.6	26.0
		-30	155	211	404.1	20.1
		0	155	200	375.3	17.7
		30	155	200	399.7	14.9
		60	155	200	403.1	18.1
		90	155	190	408.4	23.1
1000	2000	-90	155	190	400.3	22.6
		-60	155	190	288.0	59.2
		-30	155	186	142.9	64.2
		0	155	208	382.4	26.1
		30	155	208	368.8	26.6
		60	155	209	358.6	27.2
		90	155	207	339.2	37.5

Table D.3: Results - Cassie - End of Line - Table.

Fault Imp. (Ω)	Load (MW)	Inception Angle (°)	Fault Init. (ms)	Fault Ext. (ms)	Fault Mag. (A)	Post Fault Mag. (A)
10	0	-90	155	190	4239	261.5
		-60	155	188	3102	481.3
		-30	155	188	3126	371.2
		0	155	188	3183	447.6
		30	155	186	2775	430.9
		60	155	186	1918	315.9
		90	155	190	4248	55.8
10	2000	-90	155	190	3887	78.3
		-60	155	188	2167	208.0
		-30	155	189	3161	274.4
		0	155	189	6163	339.3
		30	155	189	6152	500.8
		60	155	189	3110	368.5
		90	155	190	3923	144.2
1000	0	-90	155	192	365.3	21.3
		-60	155	188	310.1	26.9
		-30	155	188	310.5	21.5
		0	155	185	314.9	19.8
		30	155	185	274.9	19.7
		60	155	186	188.3	14.4
		90	155	192	364.7	16.6
1000	2000	-90	155	193	361.0	20.9
		-60	155	186	224.9	56.1
		-30	155	188	317.7	21.5
		0	155	188	317.9	20.2
		30	155	187	317.5	19.8
		60	155	188	313.9	23.3
		90	155	190	360.2	22.9

Appendix E

Risk Assessment

The following appendix will include both a short term and long term risk analysis.

E.1 Short Term Risk Assessment

Activity/Task	Development and analysis of arcing model
Prepared By	Bradley Wentworth
Date	10-02-2016
Plant/Equipment Required	Laptop & Internet Connection

Worksafe Australia Risk Matrix

Level	Description of Consequence or Impact	Likely	Moderate	Unlikely
H (1) (High level of harm)	Potential death, permanent disability or major structural failure/damage. Off-site environmental discharge/release not contained and significant long-term environmental harm.	1	1	2
M (2) (Medium level of harm)	Potential temporary disability or minor structural failure/damage. On-site environmental discharge/release contained, minor remediation required, short-term environmental harm.	1	2	3
L (3) (Low level of harm)	Incident that has the potential to cause persons to require first aid. On-site environmental discharge/release immediately contained, minor level clean up with no short-term environmental harm.	2	3	3

Level	Likelihood/Probability
Likely	Could happen frequently
Moderate	Could happen occasionally
Unlikely	May occur only in exceptional circumstances

Step	Step Desc.	Hazards	Initial Risk Class	Controls	Residual Risk Class	Initial
1	Setup of work/study environment	Strains, slips/trips/falls	3	Use correct lifting techniques, keep area neat and tidy	3	BW
2	Research/literature review	Sore/tired eyes, sore back/neck	3	Have regular breaks (2 hours), use ergonomic chair and desk	3	BW
3	Fault modelling	Sore/tired eyes, sore back/neck	3	Have regular breaks (2 hours), use ergonomic chair and desk	3	BW
4	Reporting of results/findings	Sore/tired eyes, sore back/neck	3	Have regular breaks (2 hours), use ergonomic chair and desk	3	BW
5	Packup of work/study environment	Strains, slips/trips/falls	3	Use correct lifting techniques	3	BW

E.2 Long Term Risk Assessment

Activity/Task	Misuse of dissertation breaker failure findings (Breaker Failure timing in particular)
Prepared By	Bradley Wentworth
Date	10-02-2016
Plant/Equipment Required	N/A

Worksafe Australia Risk Matrix

Level	Description of Consequence or Impact	Likely	Moderate	Unlikely
H (1) (High level of harm)	Potential death, permanent disability or major structural failure/damage. Off-site environmental discharge/release not contained and significant long-term environmental harm.	1	1	2
M (2) (Medium level of harm)	Potential temporary disability or minor structural failure/damage. On-site environmental discharge/release contained, minor remediation required, short-term environmental harm.	1	2	3
L (3) (Low level of harm)	Incident that has the potential to cause persons to require first aid. On-site environmental discharge/release immediately contained, minor level clean up with no short-term environmental harm.	2	3	3

Level	Likelihood/Probability
Likely	Could happen frequently
Moderate	Could happen occasionally
Unlikely	May occur only in exceptional circumstances

Step	Step Desc.	Hazards	Initial Risk Class	Controls	Residual Risk Class	Initial
1	Miscommunication of Circuit breaker failure times (Too long, ie 100s instead of 100ms)	Circuit breaker failure not clearing a faulted pole in time - harm to persons and plant	1	Protection study will be undertake by utilities for each specific case - technicians will prove system grading whilst testing new settings.	3	BW
2	Miscommunication of Circuit breaker failure times (Too short, ie 1ms instead of 100ms)	Circuit breaker failure may mal operate - causing system outages	1	Protection study will be undertake by utilities for each specific case - technicians will prove system grading whilst testing new settings.	3	BW

Appendix F

Model Overview

The following appendix will include images of the overall simulink models.

F.1 Simulink Network Model - Start of Line - DT

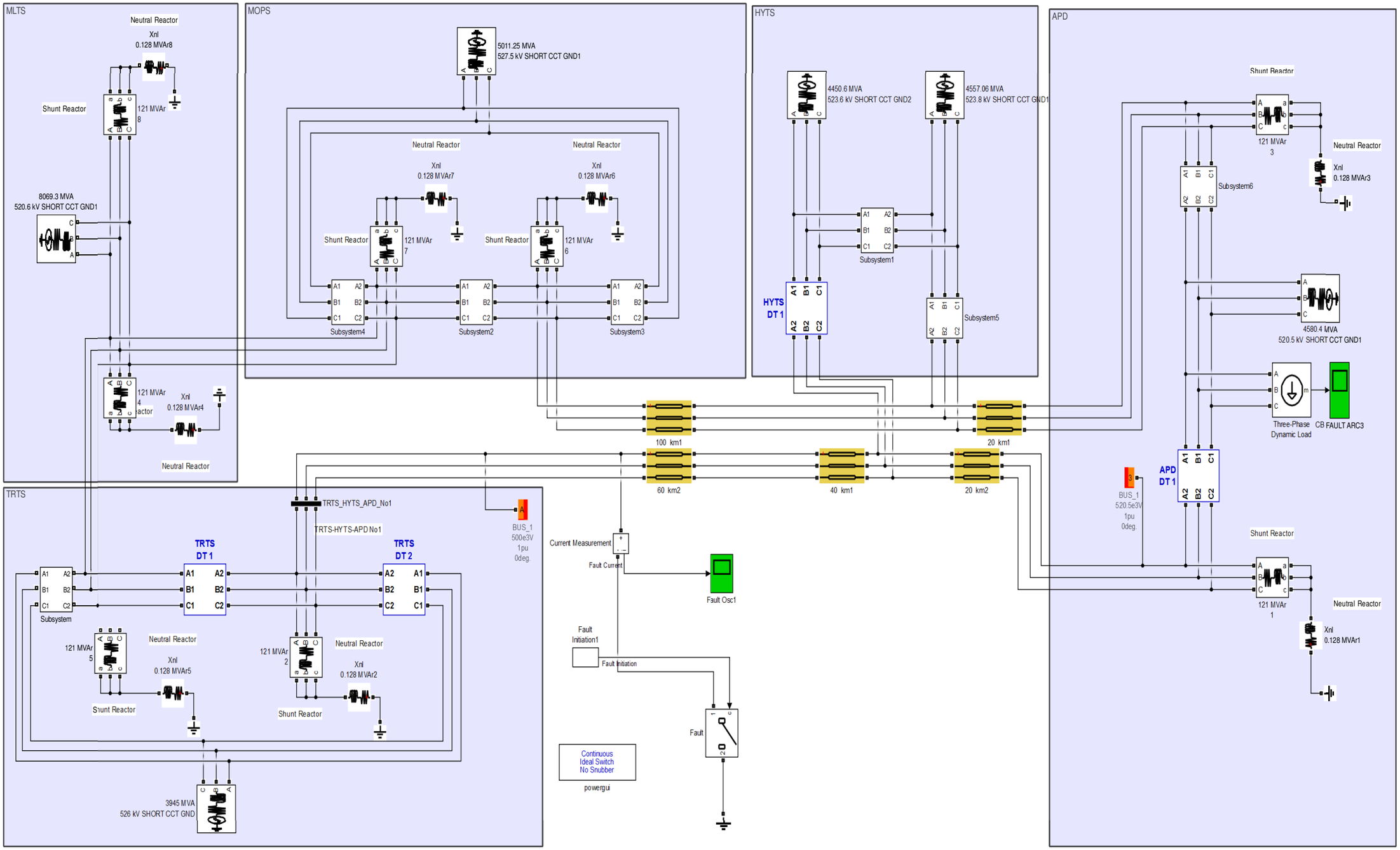

F.2 Simulink Network Model - Start of Line - Mayr

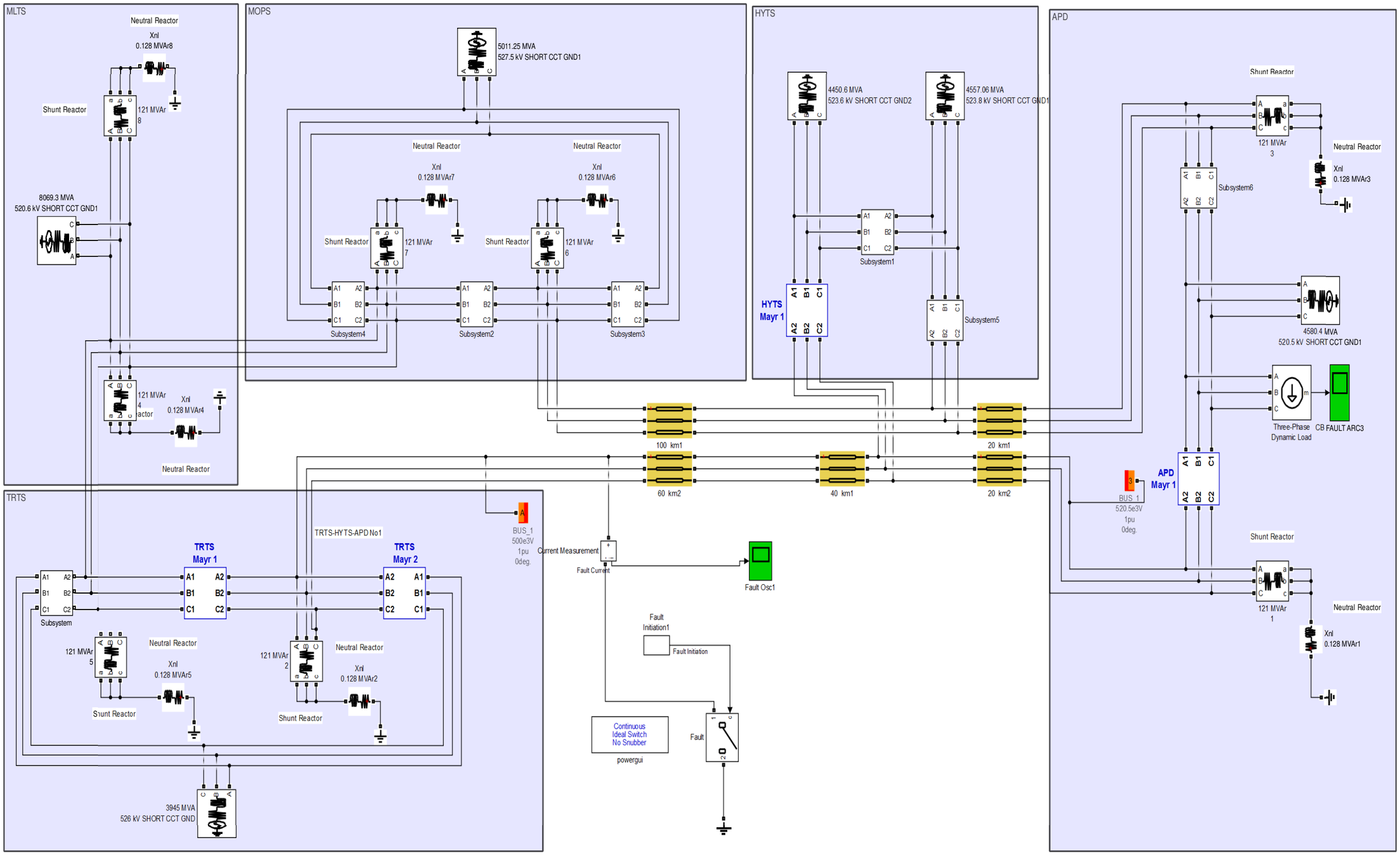

F.3 Simulink Network Model - Start of Line - Cassie

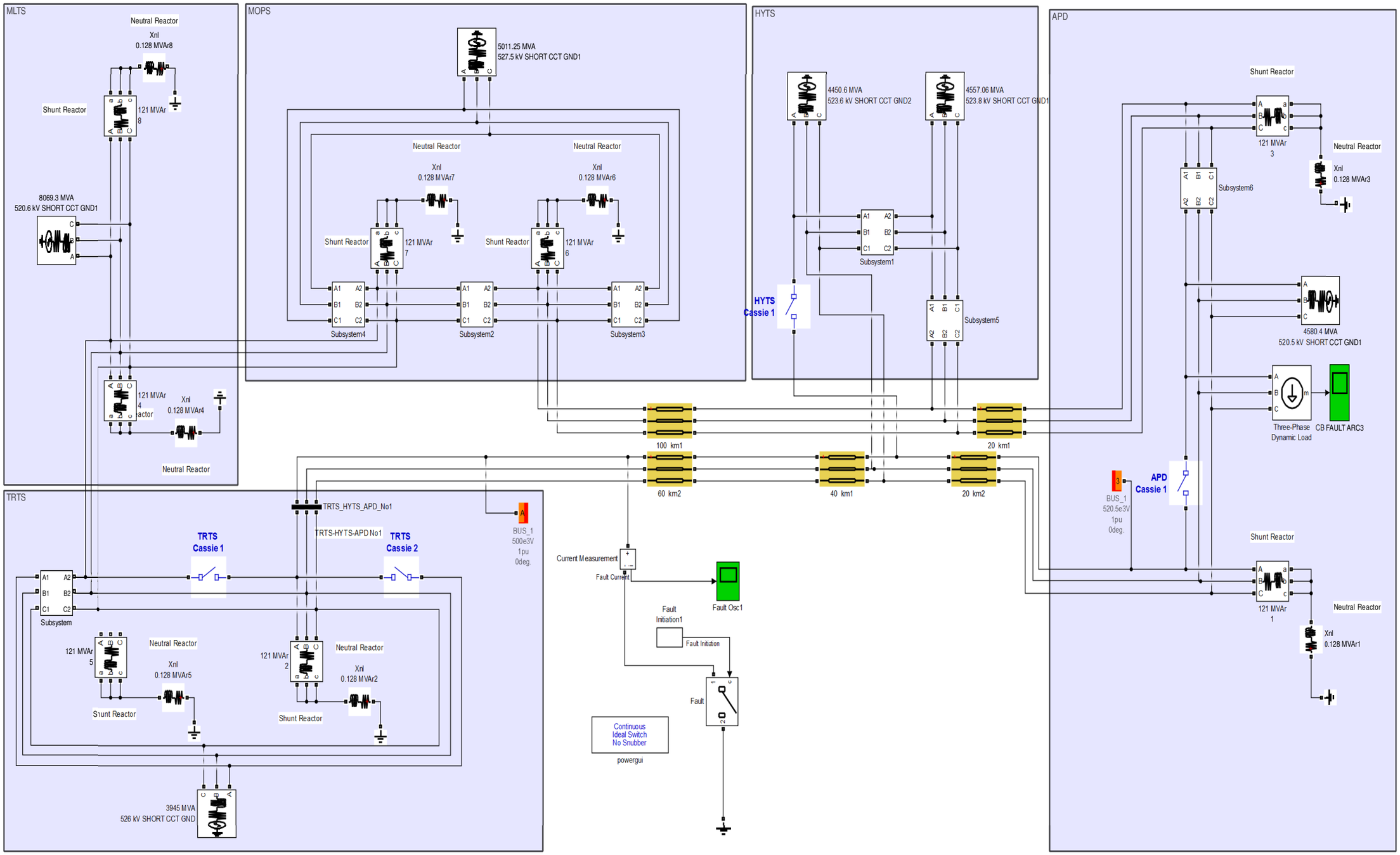

F.4 Simulink Network Model - Middle of Line - DT

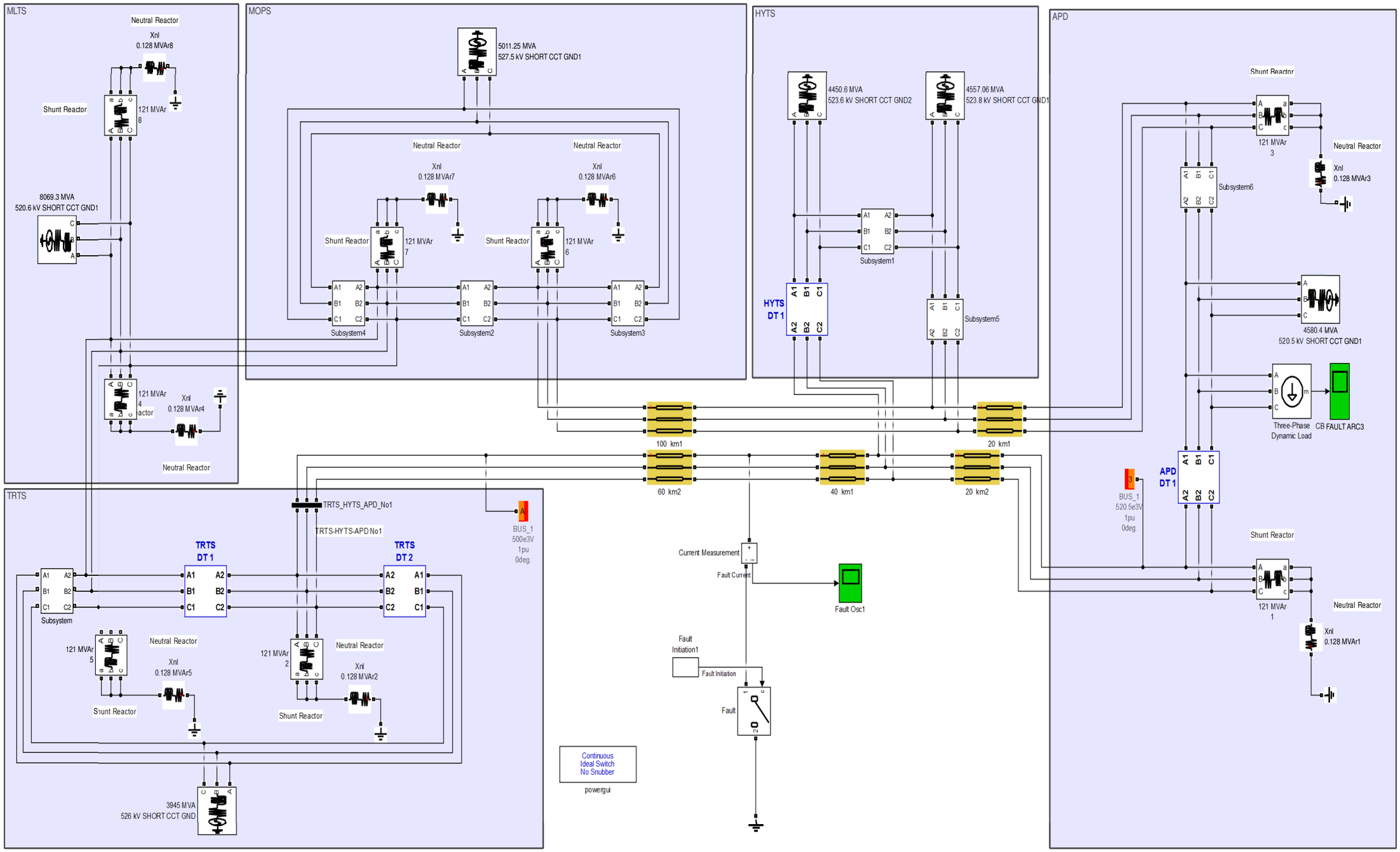

F.5 Simulink Network Model - Middle of Line - Mayr

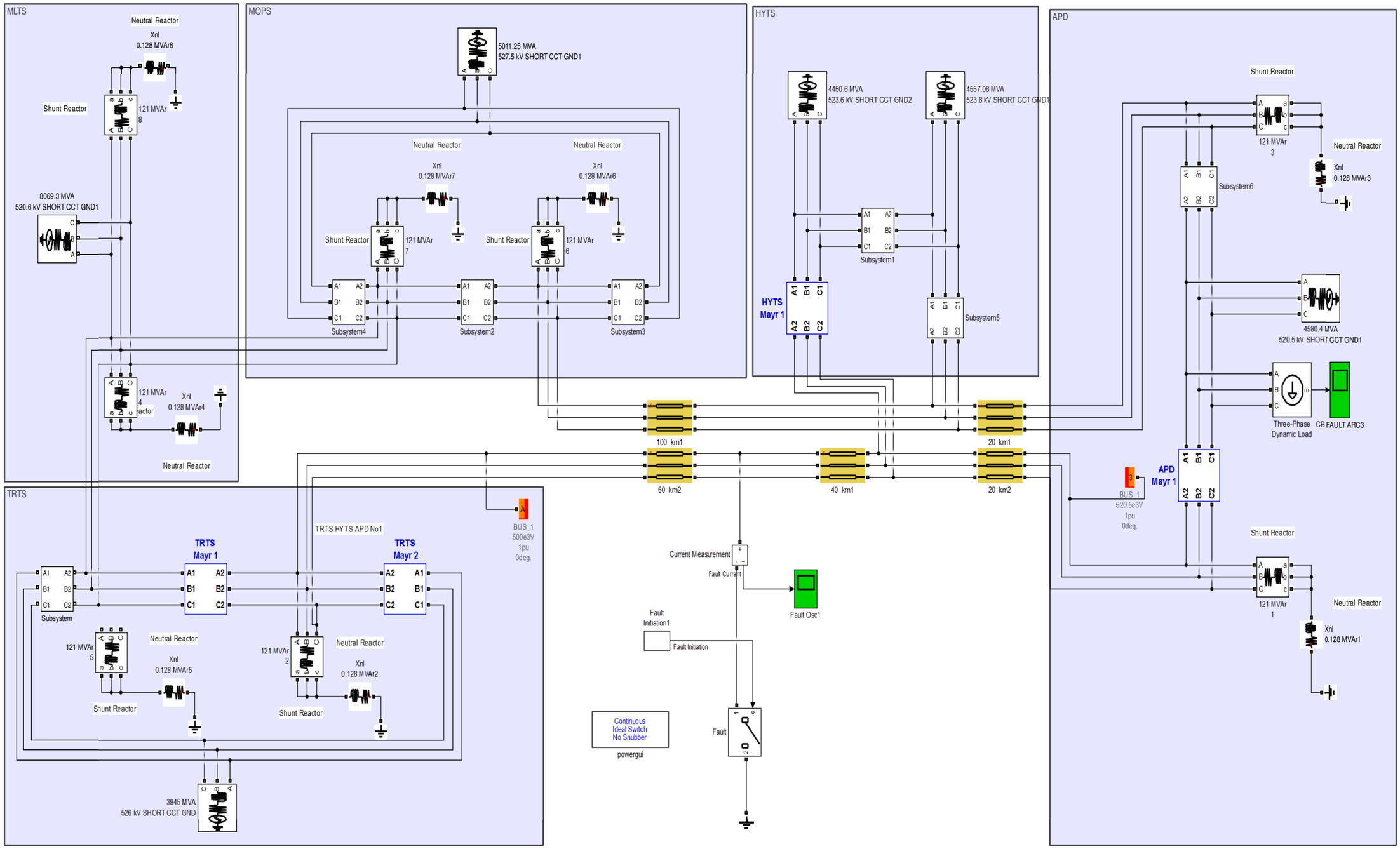

F.6 Simulink Network Model - Middle of Line - Cassie

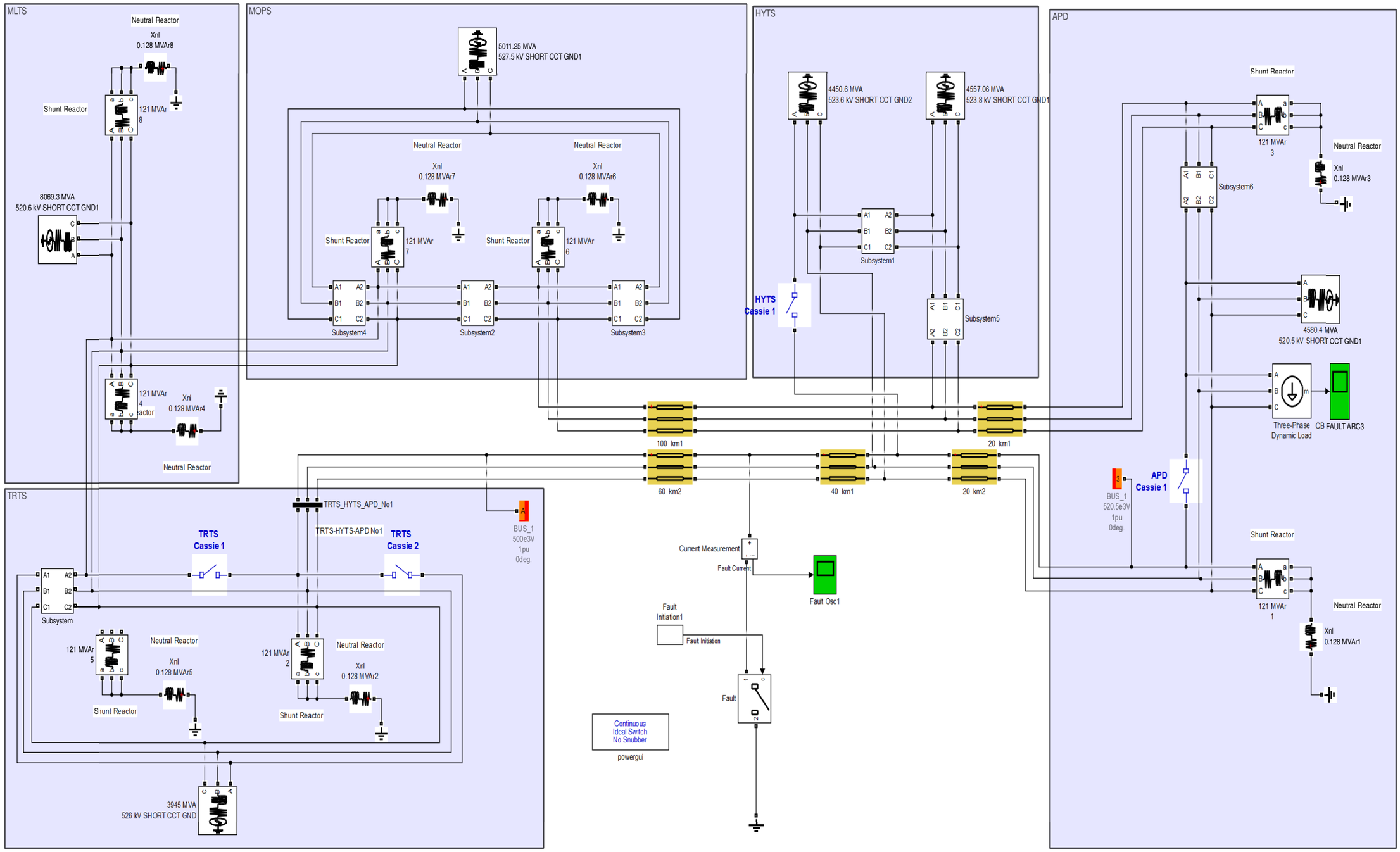

F.7 Simulink Network Model - End of Line - DT

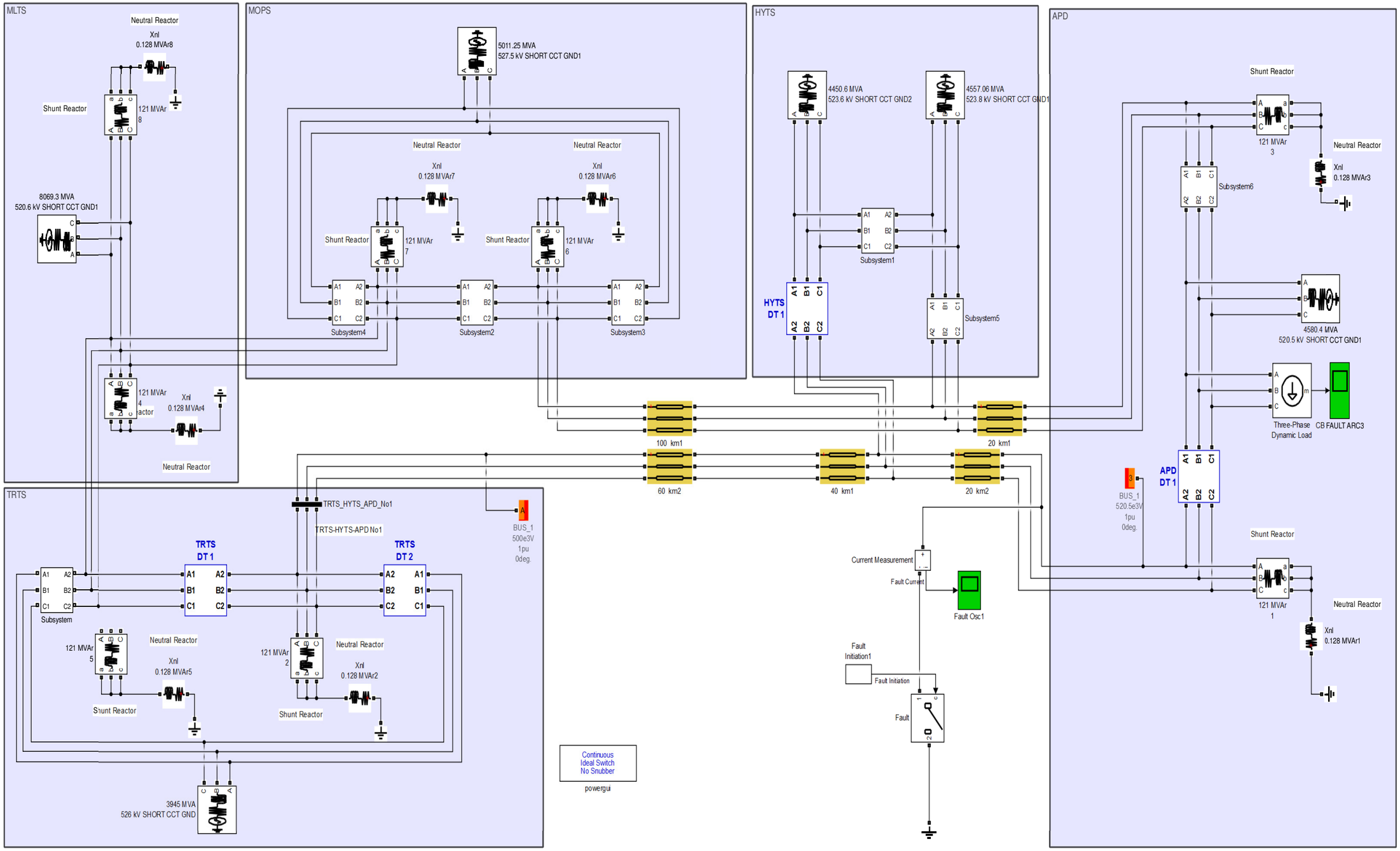

F.8 Simulink Network Model - End of Line - Mayr

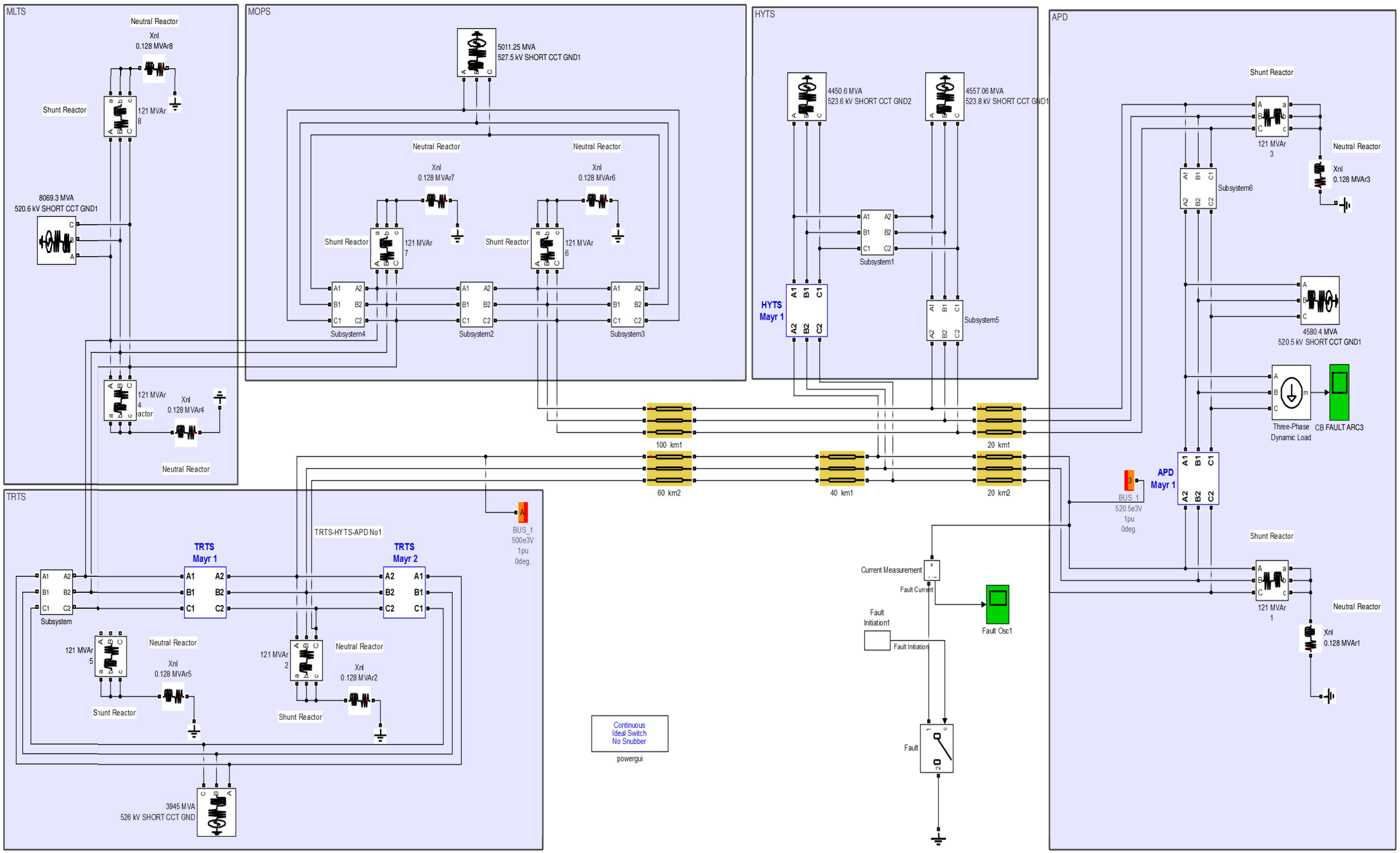

F.9 Simulink Network Model - End of Line - Cassie